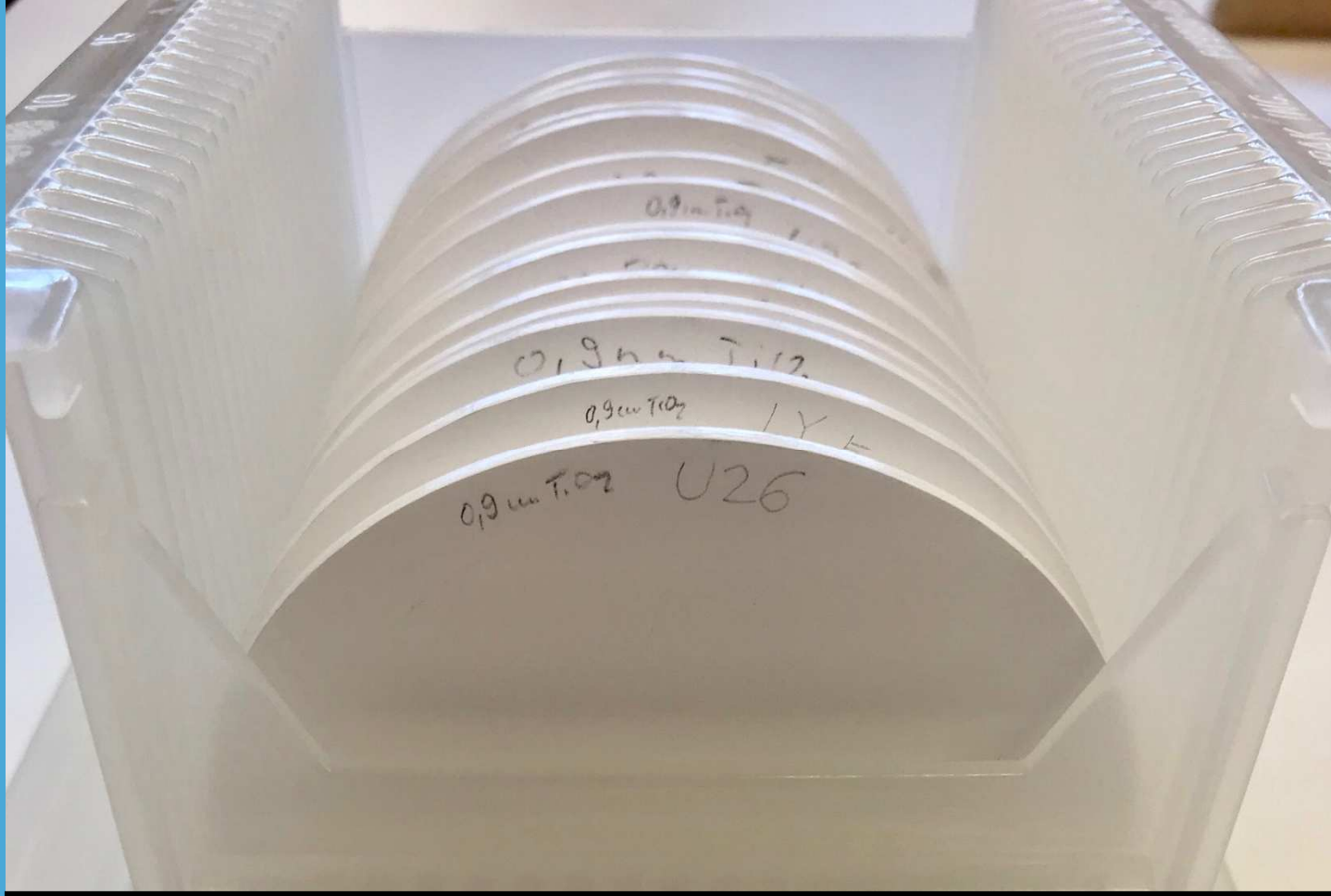

Ceramic nanofiltration membranes:
Rejection of salts and NOM at high ionic strength and modification of pore size by atomic layer deposition

Liying Feng

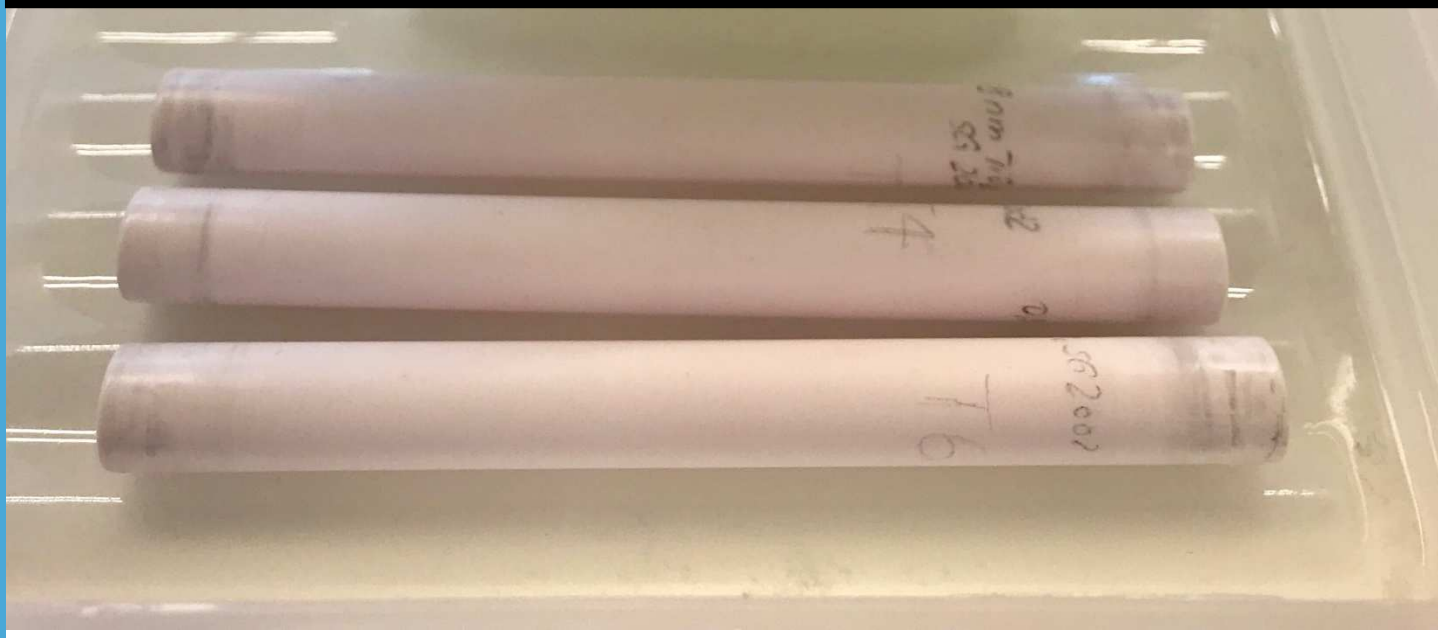

TU Delft

Ceramic Nanofiltration membranes:

Rejection of salts and NOM at high ionic strength and modification of pore size by atomic layer deposition

By

Liying Feng

In partial fulfillment of the requirements for the degree of

Master of Science
In Civil Engineering

at the Delft University of Technology,
To be defended publicly on Monday November 26, 2018

Thesis committee: Prof.dr.ir. L. C. Rietveld (Chair) TU Delft
Dr.ir. Sebastian G. J. Heijman TU Delft
Dr.ir. Ran Shang TU Delft
Ir. Irene Caltran TU Delft
Ir. Frank Dirne TU Delft

TU Delft

Kavli Nanolab Delft
Enabling nanodevice fabrication

Preface

This master thesis has been accomplished for sanitary engineering of department Water Management in the Delft University of Technology. This document is the final remark, also, the ending part of my 2 years and 4 months of MSc education in The Netherlands. This experience of studying abroad is a treasure in my life: I learnt extensive knowledge, grown up in frustration and met amazing friends. I would appreciate for all the guidance, support and encouragement that I received during the last two years.

Firstly, my deepest gratitude is to all the people who assisted me during my tough period: the last 9 months when I struggled for my master thesis. I would appreciate Professor Luuk Rietveld for giving me this opportunity to research for ceramic nanofiltration and helping me to improve my report. I also want to thank Bas Heijman for his professional suggestions for experiment and analysis throughout my research work. I am particularly grateful to Irene Caltran, my daily supervisor, who always gave me the patient guidance and enthusiastic encouragement. Without her support on arranging the experiment and constructing of final report, this thesis could not be like the current state. Many thanks to Ran Shang who gave me valuable advices on research work and warm support when I felt helpless. My gratitude also goes out to the technicians in the water-lab and kavlin lab: Armand, Mohammad and Marc, who helped me in handling the instructions.

Then, I would like to thank my friends: Rong, Simo, Yue, Mingjing. We encouraged each other in the hardest time and have so much fun in the last two years. There are so many cheerful and precious memories to look back. My fellow international student: Pui, Denise and Ravethy, who shared their experience in the company or in the laboratory with me and thank you for those.

Finally, I must express my very profound gratitude to my parents for providing me with unfailing support and continuous encouragement at every stage in my life. Without my parents, any of my accomplishment has not been possible.

Liying Feng
Delft, November, 2018

Abstract

Natural Organic Matter (NOM) is always present in the drinking water sources such as rivers, lakes and reservoirs. It causes several problems, including the unfavourable colour and odour of water, formation of disinfectant by-products and harmful microbial growth. In drinking water treatment, anion exchange (anion-IEX) is used for NOM removal. However, the regeneration of anion-IEX produces a brine, which is a high saline waste stream containing the desorbed NOM and anions (i.e. sulphate) as well as the residual sodium chloride added during the regeneration process.

One possible approach to manage the waste brine is to recover the valuable compounds from the brine, and consequently, reduce the brine volume that has to be disposed. The separation could be done by ceramic nanofiltration (NF) membranes. However, the separation performance of ceramic NF membranes at high salinity conditions is still not fully understood. Therefore, the use of ceramic NF membranes to treat the brine-like wastes that contain NOM and high salt concentrations were investigated.

Commercial 500 Dalton(Da) ceramic NF membranes were used in the salt experiments. Several experimental conditions such as pH and ionic strength were investigated to understand their influence on the rejection of sulphate (SO_4^{2-}) and chloride (Cl^-). The results show that the salt rejection was governed by charge effect, and it changed depending on pH and ionic strength. When ionic strength was 0.1M, the mitigated charge effect led to a low rejection of SO_4^{2-} (<20%) and Cl^- (<5%) by the 500Da membranes. On the other hand, the 560Da membrane used in salt&NOM experiments exhibited more than 95% rejection of NOM but less than 25% rejection of both SO_4^{2-} and Cl^- when ionic strength was 1M.

Since the 500Da membranes were unable to reject divalent ions at high ionic strength, it is suggested to decrease the membrane pore size to achieve the separation of SO_4^{2-} and Cl^-. The size of pores in ceramic membranes can be narrowed down by an approach called Atomic Layer Deposition (ALD) (Shang et al., 2017). In this study, the vacuum TiO_2 ALD was applied to coat thin films on the commercial ceramic NF membranes that have Molecular weight cut-off (MWCO) ranging from 600Da to 900Da. After the first coating, the water permeability of the membranes decreased dramatically while the MWCO of the membranes decreased slightly. After the second coating, an increased MWCO was observed, which might be attributed to the plugging of small pores. In addition, the flux distribution and pore size distribution were theoretically analysed to investigate the change of the membrane pores before and after ALD.

List of Acronyms

ALD	Atomic Layer Deposition
MF	Microfiltration
UF	Ultrafiltration
NF	Nanofiltraiton
RO	Reverse Osmosis
MW	Molecular Weight
MWCO	Molecular Weight Cut-off
PEG	Polyethylene Glycol
HPLC	High-Performance Liquid Chromatography
TMP	Tans-membrane-pressure
CVD	Chemical Vapor Deposition
GPC	Growth Per Cycle

Table of contents

List of Figures

List of Tables

1 Introduction

1.1 Ceramic nanofiltration

Clean, safe water is essential for human health, hygiene and productivity of the society. However, the water stress is expanding continually due to population growth, urbanisation and climate change. Water scarcity has become a serious issue in poverty districts. Also, the polluted water poses a threat to nature. All these circumstances indicate the importance of clean water and require the effective use of fresh water as well as water recycling (Lee et al, 2015).

In order to decline the harmful discharge and achieve sustainable water reuse, people use various methods such as chemical precipitation, biological techniques, activated carbon adsorption and membrane processes to treat contaminated water, depending on treatment purpose (Rajasulochana and Preethy, 2016). Among them, membrane process has been suggested to be the most effective and sustainable technique (Yan et al., 2016). Functioning as a barrier, membranes are capable for liquid-solid separation or gas separation. The pressure driven membrane process can be used for different treatment purposes based on their selectivity. Nanofiltration (NF) membranes, which have pore size ranging from 1 to 10 nm, offer an attractive approach to remove small organic molecules with various molecular weights from 200Da to 1000Da (Yoon, 2015). In contrast to Reverse Osmosis (RO), NF membranes need less pressure and provide higher productivity. It allows NF membranes to become one of the most favorable alternatives in inorganic ions separation such as desalination (Nicolini et al., 2016).

NF membranes are usually manufactured by two groups of materials: organic materials (i.e. polymer) and inorganic materials (i.e. ceramic) (Schaep et al., 1999). The organic membranes are attractive in large-scale applications due to their low cost and flexible configurations. At the same time, they have limitations as well. The major disadvantages of current polymeric membranes are low chemical and thermal stability, which restrict the application of organic membranes in harsh conditions (Rezakazemi et al., 2017). On the contrary, ceramic membranes have more thermal and chemical stability, as well as other advantages such as less fouling risks and high mechanical strength (Hofs et al., 2011). Thanks to unique characteristics of ceramic membranes, many studies and applications focuses on them, despite the higher production and installation costs compared to polymeric counterparts (Lee et al., 2015).

In recent years, fabrication technology has been developed for ceramic membranes. Sol-gel and solid-state sintering methods are two common fabrication technologies to prepare commercialized ceramic membranes. Both of the two process start with the formation of well-dispersed suspension or sol layer on the membrane substrate and end with a heat treatment to achieve desired selectivity (Qiu et al, 2017). Some new fabrication methods, such as fibre construction methods, the template methods and chemical deposition also been successfully applied to manufacture the ceramic membranes (Qiu et al., 2017). The core concerning in ceramic membrane fabrication is to improve the permeability, selectively and antifouling properties. Moreover, the modification methods, such as vapour chemical deposition (CVD) and ALD, are able to further tailor the membrane properties. For example,

some studies have successfully demonstrated the pore constriction by means of ALD in the ceramic membranes (Song et al., 2016). In addition, Narayan et al. (2010) used ALD to modify the surface properties of ceramic membranes and observed the antimicrobial performance of the modified membranes. The modification of ceramic membranes is becoming increasingly attractive in the research filed. With adjustable properties, the ceramic membranes can be utilized in a diverse range of industrials and suit specific filtration needs.

Ceramic NF membranes has been widely studied in terms of membrane characterizations, physical/chemical stability, rejection performance, membrane manufacturing and fabrication (Van Gestel et al., 2002, Voigt et al., 2001; Lee and Cho, 2004; Weber et al., 2003; Chung et al, 2018). In this study, we emphasised on the membrane performance for rejection of monovalent and divalent anions and NOM, together with membrane surface fabrication to modify the pore size.

1.2 Treatment of natural organic matter-rich- ion exchange brine

NOM is a complex mixture of thousands of organic compounds that occurs naturally by the degradation of plants and animal matters (Park et al., 2005). NOM is always present in surface water and groundwater. It is responsible for the colour and odour issues and need to be minimised to improve the drinking water quality in terms of avoiding the formation of disinfection by-products, guarantee of biological stability in the network and the performance of treatment processes.

Anion exchange is a commonly used technique to remove NOM during water treatment, as the main part of NOM is negatively charged (Schippers et al., 2005; Cornelissen et al., 2008). Apart from NOM, anions that are commonly occurs in raw water such as nitrate (NO_3^-), Cl^-, SO_4^{2-} and (HCO_3^-) are also adsorbed on the exchange resin after treatment. Among all the anions, SO_4^{2-} is the dominate one because most of the anion exchangers have the highest selectivity of SO_4^{2-} (Calmon, 1986; Bae et al., 2002). When the resin is exhausted, it is regenerated by (e.g.) 10% NaCl solution to recover 99.9% of the treatment capacity (Grefte et al., 2013). The regeneration process produces a high saline stream containing residual NaCl as well as desorbed anions and NOM from raw water. The waste stream from IEX containing highly concentrated salts and NOM, is referred to a brine (Drikas et al., 2011).

The disposal of the brine is a problem. The direct discharge of brine to the fresh surface water is prohibited in the Netherlands because the brine is highly saline and will make fresh water brackish. It also causes colour and odour issues in aquatic system since the organic part in brine (NOM) can act as nutrient source for growth of microbes (Texieria and Sousa, 2013). In addition, brine is too corrosive to discharge to the sewer system.

On the other hand, treatment of the brine is challenging. The main part of NOM in the brine is not readily biodegradable and thus is barely removed by biological treatment (Grefte et al, 2013). Besides, high saline brine probably gives problems in growth of microorganism. Therefore, the focus has been shifted to physical treatment techniques, especially membrane processes, which can treat brine by separating it into isolated compounds and thus reducing brine volume. The other advantage of membrane process is the relative low

energy demand compared to other physical methods that need phase change, such as vapour compression and crystallization (Ghalavand et al., 2014).

NF membranes are capable to reject organic compounds and multivalent ions. Schippers (2005) observed a good separation of humic acids from ion-exchange brine by using spiral wound and capillary NF membranes. Vaudevire and Koreman (2013) observed that NF membranes have high selectivity of SO_4^{2-} in a multi-solute system containing organic matters and salts. However, polymeric membranes were mostly used in the studies of NF membranes (Bargeman et al, 2015; Pérez-González et al, 2015; Deon, 2009; Al-Zoubi and Omar, 2009). Only few authors have worked on ceramic membranes and only the solution with low salt concentration has been considered in experiments (Khalili et al., 2015; Mazzoni et al., 2009; Condom et al., 2004). A comprehensive study on the separation of NaCl, Na_2SO_4 and NOM by ceramic NF membranes at high ionic conditions has still not been performed. Therefore, it is necessary to investigate the selectivity of ceramic NF membranes in the salt&NOM mixed system at high ionic strength. The ideal situation is that ceramic NF membranes reject organic compounds (NOM) and divalent ion (SO_4^{2-}) while let monovalent ions (Na^+ and Cl^-) to pass to make a NaCl-rich stream, which can be recycled for IEX regeneration.

1.3 Pore size reduction: Atomic Layer Deposition

It is worth noting that the membrane properties can be modified to reach a better separating performance, as described in section 1.1. One of the modifying approach is to reduce the membrane pore size in order to improve membrane selectivity. It is good to have a modified membrane with high selectively to treat the waste brine, in case that commercial membranes are not able to separate NaCl from the mixtures at high ionic strength.

ALD is considered as a promising technique for membrane modification. As a gas-phase thin film technology, ALD is known for precise thickness control and homogenous deposition. In addition, ALD is the most favourable deposition methods on high aspect structures compared to other thin film technologies (George, 2009). As mentioned above, the ALD has been successfully used to improve the membrane selectivity by narrowing the pore size of membranes.

ALD can be performed at different pressure conditions, such as in a vacuum environment or at atmospheric pressure (APALD). The vacuum ALD might be restricted in the full scale manufacturing because of the high cost of vacuum equipment (Beetstra et al. 2009). However, compared to the vacuum ALD, APALD needs more gas to purge the excessed reactants and products through the reactor, leading to a higher energy requirement. Moreover, the coating films deposited by APALD is suggested to be less homogeneous than that deposited by vacuum ALD, since vacuum is believed to prevent the formation of multilayers on the substrate surface (Beetstra et al. 2009). Shang et al. (2017) observed successful deposition of TiO_2 on the ceramic NF membranes with APALD and a reduction of pore size. However, the application of vacuum ALD of TiO_2 on the ceramic NF membranes is still a research gap. Therefore, we will focus on vacuum ALD to reduce the pore size and improve the membrane performance.

1.4 Research questions

Based on the problems mentioned above, it can be concluded that the ceramic NF membranes need to be investigated with respect to the treatment of brine-like water containing highly concentrated NOM and salts, in particular NaCl and Na_2SO_4. On the other hand, membrane selectivity can be improved by narrowing the pore size. The vacuum TiO_2 ALD, which is an approach to reduce the pore size, has not yet been applied on TiO_2-based ceramic NF membranes. Therefore, the following research questions are constructed in this study:

- What is the effect of operational parameters on the rejection of NaCl and Na_2SO_4 at high ionic strength?
- What is the influence of NOM on rejection of highly concentrated salts (NaCl and Na_2SO_4) by ceramic NF membranes? And what is the influence of salts on NOM rejection?
- Can Salts (NaCl and Na_2SO_4) be separated from salts/NOM mixtures at high ionic strength?
- How can we modify the pore size of ceramic NF membranes by approach of vacuum TiO_2 ALD?

1.5 Outline of thesis

In this study, the research focused on the separation performance of ceramic NF membranes in the treatment of solution at high ionic strength conditions, together with the modification of membrane pores to enhance the membrane selectivity. The outline of this study is structured as follows:

In chapter 2, the background theory was reviewed to understand the characteristics of ceramic membranes and their application in water treatment as well as the rejection and resistance mechanisms in the NF membranes. The membrane modification method, ALD, was also introduced.

Chapter 3 described the membrane filtration experiment. Detailed descriptions of the ceramic NF membranes, feed solution preparation and specific experimental conditions were shown. Methodologies used to evaluate the membrane characteristics (zeta-potential, water permeability and MWCO) and their rejection performance were also explained.

In chapter 4, experimental results were discussed to figure out the effect of solution chemistry such as pH and composition, and operating parameters such as cross flow velocity and trans-membrane-pressure, on the rejection of salts. The salt rejection and NOM rejection in the mixed system were studied as well. At the end of this chapter, the suggestions for membrane modification were given.

Chapter 5 described the membrane modification experiment. The vacuum TiO_2 ALD method used to coat membranes and the methodology used to evaluate the growth rate of TiO_2 were explained.

Chapter 6 showed the water permeability and MWCO of the pristine membranes and the coated membranes. A theoretical analysis was performed in the Chapter 7, in order to understand the change of flux distribution and pore size distribution of membranes after coating.

In chapter 8, the conclusions were drawn based on the results from membrane filtration experiment and membrane modification experiment. The recommendations for the further investigation were also presented.

2 Background theory

2.1 Application of ceramic membranes in water treatment

Ceramic membrane has been developed from nearly one century ago (Duscher et al., 2013). Good chemical resistance, thermal stability and high mechanical strength make ceramic membrane suitable in extreme conditions such as high temperature and high alkalinity. Therefore, they are commonly used in textile, chemical and food industry (Combe et al., 1997). The main application of ceramic membranes in the liquid filtration process is microfiltration (MF; 50nm-1um), ultrafiltration (UF; 2-50 nm) and NF (<2 nm) (Qiu et al., 2017). Each filtration process has unique applications on the basis of their separation capacity to the target compounds in terms of size, shape and molecular weight, which is illustrated in Figure.2.1.

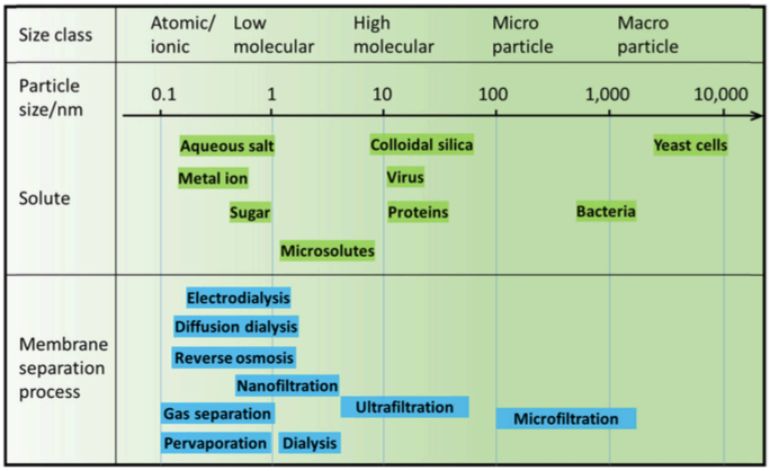

Figure 2.1 Size class of membrane filtration processes and compounds to be removed (Qiu et al., 2017)

Ceramic MF membranes have been successfully applied in industrial applications. The first commercially available ceramic MF membrane was introduced in the early 1980s, followed by the application in juice and sugar production in the late 1990s (Sondhi et al., 2003). Apart from food industries, ceramic MF membrane can also be used for oily wastewater treatment (Cui et al., 2008; Chang et al, 2014), pharmaceutical sterilization (Luque et al., 2008) or as pretreatment step for portal water production. With pore sizes in the range of 0.05-1 um, ceramic MF membranes are typically used for separation of suspended solids. The selectively of substances is influenced by fouling, pore size distribution and shape of substances (Siddiqui et al., 2016).

Ceramic UF membranes can provide higher separation performance compared to MF membranes due to the smaller pore size. In the UF process, high molecular compounds such as viruses and proteins can be retained based on the sieving mechanism together with electrostatic repulsion. Ceramic UF membranes can not only be used for purification in diary and food industries but also be utilized as concentration for protein products, including industrial enzymes and recombinant therapeutics (Khemakhem and Amara, 2012).

NF is placed between ultrafiltration and reverse osmosis (RO) according to their pore size. Ceramic NF membranes have (MWCO) between 200Da – 1000Da. Within this range, they are capable to remove relatively small macules such as dissolved salts, NOM, organic dyes and heavy metals. The application area of ceramic NF membranes includes solvent recovery and wastewater treatment. In the last decades, only a small amount of ceramic NF membranes were applied in the commercial-scale industries due to the lack of optimization experience, though many laboratory experiments have been carried out on ceramic NF membranes (Qiu et al., 2017).

2.2 Advantages and limitations of ceramic membranes

Ceramic membranes can be made from materials ranging from metal oxides (alumina, titanium dioxide and zirconia) and nonoxides (carbides, borides, nitrides, and silicides) (Luque et al., 2008). The material of ceramic membranes determines the membrane properties. For instance, they have high mechanical strength and can be applied with high flux. Due to the high flux, less membrane surface area is needed which helps to save the investment costs. With high mechanical strength, ceramic membranes can be cleaned with high pressure and velocity. Besides, Ceramic membranes can operate at high temperature and in extreme alkaline or acid environments. It allows ceramic membranes to be cleaned with aggressive chemicals or hot streams (Benfer et al, 2011). The excellent properties of ceramic membranes make them essential for many applications where polymeric membranes can not be used. Last but not least, ceramic membranes are able to offer reliable treatment performance over a long period of time and they can be recycled.

Ceramic membranes also have limitations. One of them is the high costs, which is a combination of expensive material and high manufacturing costs. The price of commercially available ceramic membrane is ten times higher than that of polymeric counterparts (Ciora et al., 2003). Also ceramic membranes suffer from defects, which can be caused by a clash with membrane holders (Shang, 2014). In addition, sealing can be vulnerable, as Kramer et al (under review) showed that the sealing of commercial membrane was not chlorine-resistant.

2.3 Structure and configuration of ceramic membranes

2.3.1 Structure of ceramic membranes

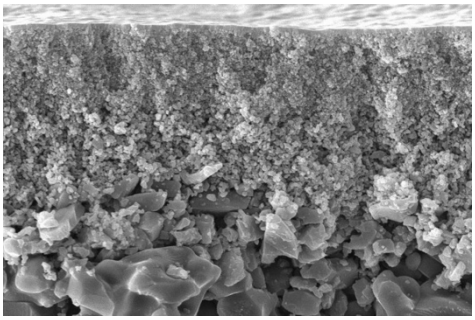

Figure 2.2 SEM image of the ceramic membrane on the cross section (Inopor® membranes)

In general, ceramic membranes have asymmetric structures that compose of a support layer, intermediate layers and a separation layer (Erdem, 2017; Fan et al., 2016). The Support layer is mainly responsible to provide mechanical stability and strength for the overall membranes. The layer with the finest pore size is called separation layer where the separation in fact takes place. Between the support layer and the separation layer there are multiple layers, called as intermediated layers, serving as a bridge. The pore size within this layer gradually narrows from support layer towards top layer, which is illustrated in Figure 2.2.

2.3.2 Configuration of ceramic membranes

a (Amin et al., 2016) ***b*** (Sxceramic, 2018) ***c*** (Cleanflow, 2018)

Figure 2.3 Ceramic membranes in different configurations (a)plate (b) tubular (c) hollow fibre

Plate membranes

Plate membranes are also called pillow-shaped membranes (Amin et al., 2016). The contaminated water flows through the top layer towards the support layer of the plate membranes. When treatment is completed, the permeate can be collected and carried away by drains. Within a module, multiple disk membranes can be packed together in one unit with a certain distance, which helps to increase packing density of the membrane module and save costs per module (Baker, 2004).

Multi-channel membranes

Multi-channel membranes have high surface area/volume ratio. In addition, it is easy to increase surface area by increasing the number of channels in the membrane without changing its outer diameter. The multi-channel membranes are typically characterized by high packing density, which makes them suitable in full-scaled applications.

Hollow-fibre membranes

The ceramic membrane can be manufactured into capillary shape. Numerous membrane capillaries are potted in a module as a whole to be used in practical applications. Although hollow fibre membranes have extremely large surface area, this advantage is often offset by their low flux.

2.4 Membrane characterization

2.4.1 Water permeability

Water permeability of membranes is important in industrial applications because it characterizes the productivity of membranes and helps to predict the specific energy required to generate permeate (Merdaw et al., 2010). In general, higher membrane selectivity leads to a lower water permeability (Li et al., 2018). However, it should be noted that the water permeability is not only determined by pore size, but also by the thickness, porosity, tortuosity and hydrophilic/hydrophobic properties of membranes (Kim et al., 2010). For asymmetric membranes, composed of different layers (skin layer, intermediate layers and supporting layers), the contribution of each layer to the water permeability might be different, as they can be fabricated by different techniques and made from various materials.

The water permeability of commercial membranes can be changed by additional manufacturing procedures such as dip-coating and ALD. The water permeability of membranes after manufacturing decreased (Karnik et al, 2003; Chen et al, 2018; Li et al., 2016) or increased (Nerweij et al., 2007) depending on the substrate membrane, manufacturing techniques and deposited materials used in the studies.

2.4.2 Pore size distribution

The pore size of NF membranes is not homogeneously distributed. Both larger pores and smaller pores exist in the membrane. The proportion of larger pores and smaller pores (or pore size distribution) affects the membrane performance in terms of permeability and selectivity (Siddiqui et al., 2016). Therefore, it is important to know the complete pore size distribution when characterizing the porous membranes.

A narrow pore size distribution refers to the situation that all pores are of similar size, whereas a broad size distribution means that there are a large number of smaller pores and a small number of larger pores (Cao et al., 1993). Literature suggests that a narrow pore size distribution provides a stable permeate production with desired quality (Shang, 2014), and a broad pore size distribution deteriorates the membrane performance and increases the risk of fouling (Siddiqui et al., 2016; Yoon, 2015).

The pore size and its distribution can be measured by N2 adsorption/desorption experiments, or other measurements from water/liquid or gas permeability (Calvo et al., 2008). For instance, by measuring the fractional rejection of nonionic polyethylene glycol (PEG), one can determine the pore size distribution of a membrane through a relation between solute rejection and solute size (Lee et al., 2002). Figure 2.4 gives an example of the narrow pore size distribution and broad pore size distribution by plotting the rejection curves from PEG rejection experiments.

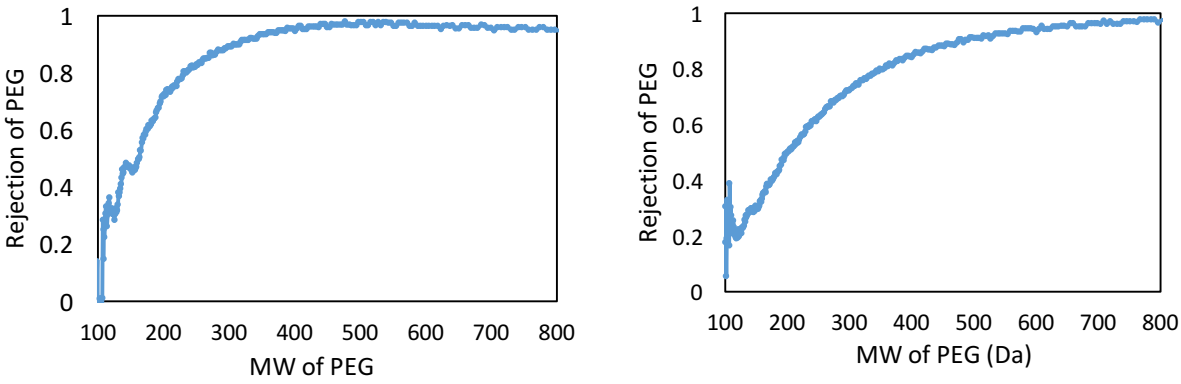

Figure 2.4 Narrow pore size distribution (A) and broad pore size distribution (B). (data source: Shang et al., 2017)

2.4.3 Defects

Defects are breakage and deficiency of the membrane structure, or large pores with sizes far beyond the range of normal pore sizes, such as, the mesopores in a microporous membrane (Koutsonikolas et al., 2010). Defects can be formed during membrane preparation (i.e. the drying phase during sol-gel process) and during the filtration process (i.e. the extrusion from membrane holders) (Shang, 2014). For NF membranes, the defects, even in the nm range, facilitates the passage of large compounds through membranes, and deteriorate the selectivity of membranes dramatically (Koutsonikolas et al., 2010). Therefore, producing a defect-free membrane is essential to maintain a high membrane performance.

2.5 Retention mechanisms in NF membranes

2.5.1 Sieving effect (steric exclusion)

Steric exclusion is determined by the size of membrane pores and the size of compounds in the liquid. If the compound has a smaller molecular size than the size of the membrane pores, it can permeate through the membrane, while the compounds having a lager molecular size than the size of membrane pores are rejected.

The MWCO is typically used to predict the rejection capacity of porous membranes. The MWCO of a membrane is defined as the molecular weight of uncharged molecules which are retained by 90%. The organic molecules such as PEG and proteins are used to measure the MWCO. However, the free space inside membranes and component shape are not uniform, which means that smaller molecules can also be retained by geometrical shape (Salmenhaara, 2016). This might lead to an overestimation of MWCO.

2.5.2 Charge effect (electrostatic repulsion)

The effect of membrane charge on ion transfer has been described by Donnan and it is based on the Donnan equilibration theory (Donnan, 1995). According to this theory, the movement of ions through a semi-permeate membrane is a result of electro equilibration. When a negative charged membrane is in contact with solutions containing both anions and

cations, cations are attracted by the negative charged species on the membrane surface and tend to travel towards to the membrane surface. Meanwhile, anions are repelled and move to the bulk solution, decreasing their concentration near the membrane surface. This phenomenon is illustrated in Figure 2.5.

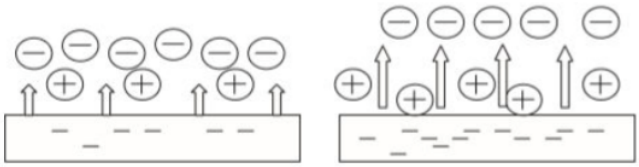

Figure 2.5 Schematic illustration of charge effect for the negative charged membrane

The electrostatic attraction or exclusion can be weak or strong depending on membrane charge and ion valence of the solutes. On the charged membranes, the electrostatic force of multivalent ions is higher than that of monovalent ions. It is also easily understood that membranes with a greater charge have a higher retention of co-ions (ions of same charge as charged surface) than the membrane with less charge.

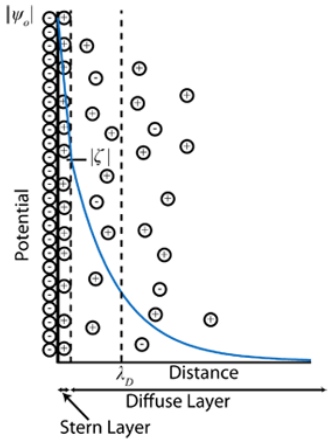

Figure 2.6 Electrical double layer near the negatively charged surface and potential decreasing along the distance form wall to bulk solution (Web.mit.edu, 2018)

Surface charge characteristic of membranes is commonly described by zeta-potential (Hurwitz et al., 2010). When membranes are immersed in electrolyte solution, due to dissociation of functional groups or adsorption of ionic surfactants, charge is accumulated on interface of membranes and aqueous electrolytes and forming electrical double layer (Schäfer et al., 2005, Tadros, 2014). An electrical double layer consists of a monomolecular Stern layer that exists next to the membrane surface, and an incompact diffuse layer that occurs in between the stern layer and bulk solution. The potential in the double layer decays along the distance from the surface to the bulk solution (Figure 2.6). The potential difference between the surrounding dispersion medium and the stable medium that is attached to the surface is known as zeta-potential (Kulkarni, 2009). In membrane technology, zeta potential reflects the charge characteristic of membranes and is related to

the electrostatic repulsion. Zeta potential can be alerted by solution chemistry, such as pH, ionic strength and temperature (Skluzacek et al., 2007).

2.5.3 Dielectric exclusion

Dielectric exclusion is caused by the difference of the dielectric constant between membrane matrix and adjacent electrolyte solution (Zhao and Li, 2006; Vezzani and Bandini, 2002). Dielectric exclusion can be explained with a series of concomitant effects. The difference of dielectric constants leads to electrostatic interactions between ions and polarization charges induced by ions at the dielectric boundary. The ion induced charge has the same sign as the ions in the media, which causes an additional repulsion mechanism (Vezzani and Bandini, 2002). Moreover, the dielectric property of the charged ions alters inside the membrane pores compared to that in the bulk solution due to the changes of the solvent structure. Polar solvents which are randomly orientated surrounding ions change the orientation order in the narrowed membrane pores (Figure 2.7), increasing ion solvation energy and creating extra repelling force (Szymczyk and Fievet, 2006; Déon et al., 2009).

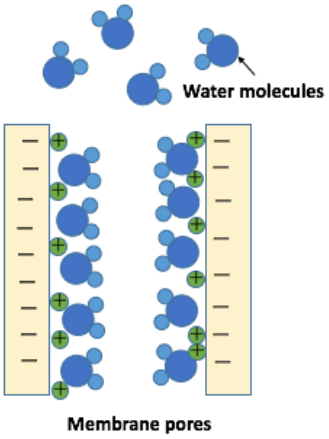

Figure 2.7 Motion of water molecules when entering into membrane pores

It is reported that a rejection of divalent ions, such as Mg^{2+} and Ca^{2+}, was well predicted with the model in which dielectric exclusion was taken into account as an additional partitioning effect (Szymczyk and Fievet, 2006). However, dielectric exclusion is not evident in the case of a mixtures containing various co-ions and with rejection of monovalent counter ions (Vezzani and Bandini, 2002, Silva et al., 2016). Bandini and Vezzani (2003) and Pérez-González et al (2015) worked with NaCl-Na_2SO_4 mixtures on NF membranes in models and they concluded that dielectric exclusion was not relevant in determining salt rejections in NaCl-Na_2SO_4 mixtures, especially with a high ionic strength (Pérez-González et al 2015). It means that in this study where highly concentrated mixtures of NaCl-Na_2SO_4 were used, only the classic theories (steric effect and donna effect) were suitable to describe ion transport in NF membranes.

2.5.4 Convection and diffusion

Besides electromigration, convection and diffusion are two dominant mechanism involved in ions transport through porous membranes (Schaep et al., 1998). The convection of liquid is caused by a pressure gradient while the diffusion is caused by a concentration gradient (Schaep et al., 1999). Convection and diffusion have different contribution to ions transport

under different conditions. Szymzyk et al. (2003) concluded that convection dominates electrolyte transport at low membrane charge density and high permeate volume flux, whereas the transport is governed by diffusion when membrane is strongly charged and at low permeate volume flux. According to Sagle and Freeman (2004), the pressure driven convection effect is much more significant than the diffusion through the UF and MF membranes. In NF membranes, convection governs the transfer of divalent ions (i.e.SO_4^{2-}), while diffusion is the dominate mechanism in controlling monovalent movement (Sagle and Freeman, 2004, Kelewou et al., 2011).

The diffusion mobility of specific species is indicated by the diffusion coefficient, also called diffusivity. The diffusion coefficient is depended on temperature as well as the transporting media. A typical diffusion coefficient for a molecular dissolved in aqueous solution is between 10^{-10}m/s and 10^{-9}m/s (comsol, 2018). The higher the diffusivity of species, the faster they diffuse through barriers. Convection of species, on the other hand, is governed by flux. In membrane filtration, the driving force for convection is trans-membrane pressure (TMP), which is positively proportional to the permeate volume flux.

2.5.5 Hydration

Hydration plays an important role in rejection of ions regarding to the mechanism of size exclusion. Hydration occurs in an aquatic solution between water molecules and charged ions. In the aqueous solution, ions tend to electrostatically attract vicinal water molecules. Since water molecules are asymmetrical and slightly polarized, they arrange themselves around ions and form a hydration shell as illustrated in Figure 2.8. Therefore, the ions exhibit a larger radius in an aqueous solution than its crystallographic radius.

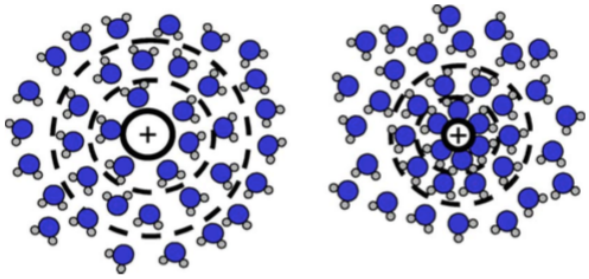

Figure 2.8 Illustration of hydration shell for large and small ions. The circles represent hydration shell (Tansel et al., 2006).

Hydrated radius is depended on crystallographic radii and charge density of the central ions (David et al., 2001). Havel and Högfeldt (1995) concluded that smaller ions have stronger bonds with water molecules than larger ions (Figure 2.7). Ions with more charge density hold larger water clusters than ions with less charge density. Besides, the hydration shell is more compacted around anions than the cations for the same charge density, indicating the smaller hydration radius of equal anions (Tansel et al., 2006). Environmental factors such as pH, ionic strength and temperature also influence the strength of hydration (Tansel et al., 2006).

During the filtration process, dehydration might occur on the ions with a loose hydration shell. Some or all of the weakly bonded water molecules will disconnect to central ions. Ions losing water molecules become smaller and can permeate through membranes. On the contrary, ions with strong hydration bound might be repelled by membranes due to the large size.

2.6 Resistance mechanisms in NF membranes

2.6.1 Concentration polarization

Concentration polarization always occurs in NF and RO, and it is caused by accumulating solutes adjacent to the membrane surface (Bian et al., 2000). Figure 2.9 illustrates the mass transfer system in a cross-flow filtration mode at steady state. During filtration both solvent and solutes are forced towards the membrane by water flux. However, the solutes which are retained by size exclusion and electrostatic repulsion accumulate near the membrane surface. Consequently, the concentration of solute on the membrane surface is higher than in the bulk solution, resulting in back-diffusion of solute (the solute moves away from the membrane surface). The competition of the convective force to the permeate side and the back diffusive force determines the concentration distribution at a steady state. The region where solute concentration varies spatially near the membrane surface is indicated as concentration polarization layer (Bhattacharjee, 2017).

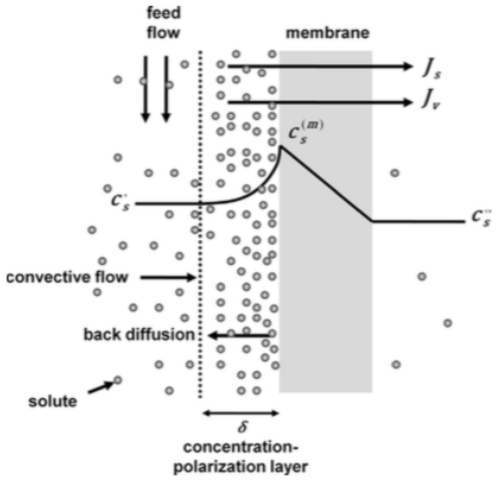

Figure 2.9 Mechanism of solutes transport through concentration polarization layer and membrane (Pages et al., 2013)

Concentration polarization causes serious problems in membrane filtration. With concentration polarization, the osmotic pressure of solution increases on the region near the membrane surface (Winter et al., 2017). When the osmotic pressure increases, the effect of the driving force decreases, and this causes flux decline. Moreover, the observed rejection of solute is lower due to the lower permeation rate of the solvent. Potential disadvantages of concentration polarization such as the scaling and increased risk of fouling are also reported (Ahmed, 2013). In order to reduce the negative impact of concentration polarization, it is suggested to use cross flow filtration rather than dead end filtration. In cross flow filtration, the flow parallel to membrane sweeps the accumulated solute on the membrane surface and therefore helps to reduce the thickness of boundary layers. During

dead end filtration, the thickness of boundary layer is infinitely large. It should be noted that concentration polarization can only be mitigated but never be eliminated during filtration (Halem et al., 2009).

2.6.2 Fouling

In membrane-based filtration, the retained substances continuously increase the resistance of membranes and cause flux decline. This unfavorable phenomenon is called fouling. Fouling is associated with the adsorption and accumulation of foulant inside the membrane pores or on the membrane surface (Mustafa et al., 2016). The foulant materials can be inorganic compounds, organic matter or microbes. The dissolved fraction of foulant and growth of microbes within membrane pores are major contributors to irreversible fouling, which can only not be removed by chemical cleaning (Sun et al., 2013; Yaldız, 2017). If the foulant can be removed by hydraulic backwash, this type of fouling is known as reversible fouling. The flux decline due to fouling is different from flux decline due to concentration polarization; fouling causes long term flux decline, while concentration polarization causes fouling that does not increase with time (Fig 2.10).

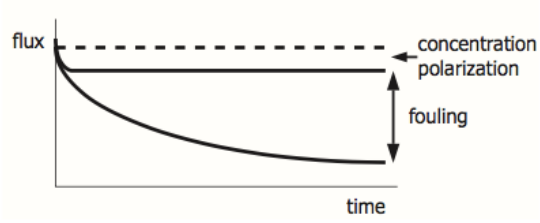

Figure 2.10 Concentration polarization and fouling with time in cross flow filtration (Halem et al., 2009)

The extent of fouling is determined by operating conditions (i.e. recovery, flux and cross flow velocity), feed water quality and membrane properties (i.e. roughness, porosity, material and surface chemistry) (Mustafa et al, 2016). Several studies have suggested that ceramic membranes are less sensible to a fouling compared to polymeric membranes (Hofs et al., 2011). Lee and Kim (2014) observed lower fouling tendency of ceramic membranes than with polymeric counterparts during NOM filtration; and they attributed this to the hydrophilic properties of ceramic membranes, resulting in less adsorption and weaker interaction between ceramic membranes and NOM. Lee (Lee, 2013) used filtration models to investigate fouling characteristics of membranes, and reported that ceramic membranes exhibit less irreversible fouling than polymeric membranes.

2.7 Membrane modification: Atomic Layer Deposition

2.7.1 Application of ALD in membrane modification

ALD is an attractive technique for membranes fabrication and modification. It is able to coat thin films of polymer, metal and oxides and other materials on ceramic or polymeric membranes in a wide range of processing temperature (Li et al., 2012). In recent years, there are a number of studies on utilizing the ALD to modify or functionalize the membranes. Chen et al. (2018) used TiO_2 ALD to constrict the pores of ceramic membranes from ultra-level to nano-level for an effective separation of dye from wastewater. Nikkola et al. (2014)

presented membrane modification by trimethylaluminium ($AlMe_3$) ALD on the RO polymeric membranes to improve their anti-fouling performance. Li et al. (2011) observed that ALD techniques are capable of reducing the pore size of polymeric membranes, and of modifying their surface physicochemical properties (i.e. hydrophilicity). Numerous successful applications of ALD on membranes has been demonstrated in the research filed and attention to ALD is still growing. However, the complex process and expensive ALD equipment limit the application of ALD for membrane preparation on a large scale (Weber et al., 2018). Currently, the effective and cheaper ALD is being developed to increase the throughout of deposition, consequently creating the opportunity for industrial applications (Weber et al., 2018).

2.7.2 ALD process

The gas-phase ALD coats continuous and uniform layers by self-limiting reaction. Figure 2.11 illustrates a type cycle of ALD in the reactor. A precursor is pulsed to the substrate surface for a certain amount of time to allow a full reaction with surface groups. This is followed by a pump or purge phase to remove unreacted precursors and by-products. Consequently, the co-reactant reacts with the first precursor, forming a binary thin film. The purge is conducted again in the end to finish one cycle. As this reaction proceeds continuously, multi-layers can be deposited on the substrate surface. the first precursor is typically a metal-centred compounds surrounded by functional groups, while the co-reactant can be water vapour or oxygen gas (Weber et al., 2018). It is obvious that the precursors and co-reactant on each cycle affect the ALD process. Moreover, the physical parameters in ALD, including operating temperature, pressure, purge time and pulse time, also have a profound influence on the conformality of deposited thin films (Johnson et al., 2014).

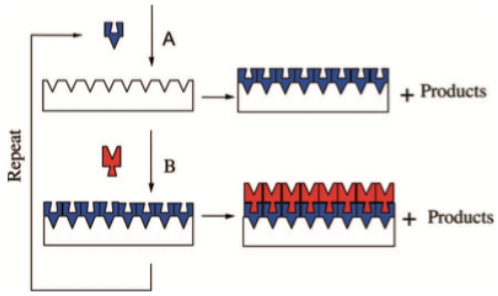

Figure 2.11 Schematic illustration of the sequential, alternating self-limiting surface reactions. A: the first precursor B: the second precursor (co-reactant) (George, 2009)

3 Membrane filtration: materials and methods

3.1 Ceramic membranes and membrane holders

Commercial ceramic NF membranes used in this laboratory-scale study were provided by Inopor (Inopor GmbH, Germany). According to the manufacturer, the ceramic NF membranes have a porosity of 30-40%. They consist of a porous support body of Al_2O_3 with a pore size of about 3 µm, several intermediate layers with smaller pore size and a separation layer of TiO_2 with mean pore size of 0.9 nm prepared by sol-gel methods (Inopor, ceramic nanofiltration membranes).

Single-channeled tubular membranes and flat disc membranes were used in this study. The tubular membranes have channel diameter of 7mm and an outer diameter of 10mm with a length of 75mm. The effective filtration area of the tubular membranes is 0.00163 m^2. The disc-shaped membranes have an effective filtration area of 0.0056m^2, with a corresponding diameter of 0.0084m. Apart from the configurations and dimensions, the other characteristics of the two types of membranes (i.e. selectivity and surface charge) were considered to be the same, as they were manufactured by the same procedure and made from the same materials.

The filtration experiment was done in an inside-out mode for the tubular membranes and in tangential mode for the disc-shaped membranes. The tubular membranes were operated in a PVC module (Figure 3.1a). The maximum operating pressure of the PVC module is 10bar. The disc membranes were operated in a disc-holder (TAMI Industries, France) (Figure 3.1b) made of stainless steel, with a maximum operating pressure of 4bar. Therefore, the tubular membrane and plastic module were used when a pressure higher than 4bar was required in the filtration experiments.

(a) ***(b)***

Fig 3.1 Pristine ceramic membranes with different configurations and corresponding membrane holders

3.2 Experimental set-up

Two similar cross-flow systems were used for the filtration tests. Figure 3.2 shows a schematic overview. The feed tank contains a solution (ultrapure water, PEG or salt solutions), which was pumped to membrane module. In the cross-flow membrane module, the feed flow was separated into a permeate flow and a concentrate flow. A small amount of the permeate was collected for further analysis, while the rest of the permeate and the concentrate were recycled continuously into the feed tank. Two pressure meters were

placed on two sides of the membrane module, measuring the pressure of the feed flow and the concentrate flow. The temperature and pH in the feed tank were measured by a pH meter (Xylem Analytics Germany GmbH, Germany). A flow meter was used to monitor the pump flow. The cross flow and TMP were regulated by adjusting the pumping speed and the concentrate valve.

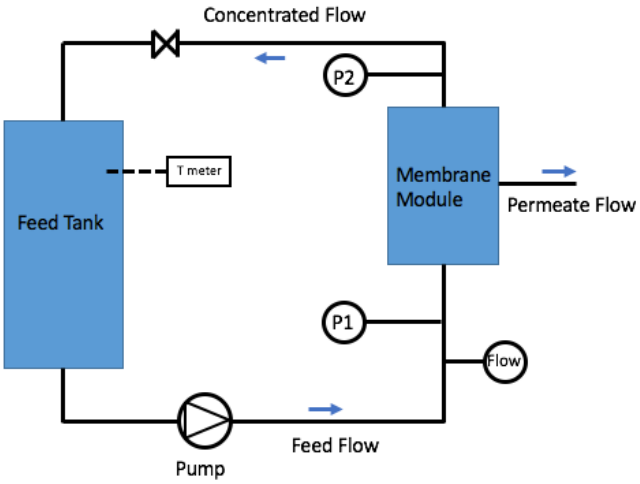

Figure 3.2. Schematic Overview of Experimental set-up

3.3 Membrane cleaning

After salt filtration or PEG filtration, the permeability of the membrane decreased. Therefore, the membranes were cleaned chemically. To perform chemical cleaning, the membranes were immersed in a 0.2% sodium hypochloride (NaClO) solution for 2 h (after PEG filtration) or 0.5h (after salt filtration), followed by 0.5h immersion in ultrapure water to remove the residual chemicals on the membrane surface. After cleaning, the water permeability of the cleaned membrane was tested again. If the recovery of the water permeability was too low, the cleaning process was repeated until the water permeability came close to the original permeability.

3.4 Membrane characterization

3.4.1 Water permeability

Ultrapure water was used to test the water permeability of the membranes. The experiment was carried out under room temperature (~28℃) at a constant TMP of 3±0.2bar. The cross flow velocity was set at 7 m/s and 1.3 m/s for disk membranes and tubular membranes respectively. The weight of permeate was measured automatically in every one minute by a balance (KERN, Germany). The reading of temperature, TMP and cross flow were recorded manually three times during 20-minute measurement period. Due to external energy from the running pump, the feed water was heated up during filtration process. Therefore, a temperature-corrected equation was used to calculate the ultra pure water permeability; this is shown in Equation 3.1 (Shang et al., 2017).

$$L_{p,20℃} = \frac{J}{\Delta P} \cdot \frac{\eta_T}{\eta_{20}} = \frac{J \cdot e^{-0.0239(T-20)}}{\Delta P} \qquad Eq.3.1$$

$$J = \frac{Q}{A} \qquad Eq.3.2$$

Where $L_{p,20℃}$ is permeability at 20℃ in $m^3/(m^2 \cdot s \cdot bar)$; J is measured flux in $m^3/(m^2 \cdot s)$; T is measured temperature in ℃; ΔP is TMP in Pa; η_T is permeate viscosity at measured water temperature and η_{20} is permeate viscosity at 20℃. Q is the permeate flow rate in L/h; A is effective filtration area in m^2.

3.4.2 Molecular Weight Cut-off

Sample collection and analysis

The feed solution used for MWCO measurement contained a mixture of PEG (SIGMA-ALDRICH, Germany) with various molecular weight (200Da, 300Da, 400Da, 600Da and 1000Da). The concentration of each PEG was 0.6g/L. The experiment was started with a stabilization period of 50min filtration, after which the permeate sample and feed samples were collected in a time interval of 10min. Meanwhile, temperature, cross flow and TMP were recorded three times to calculate the average permeability. The total filtration period was 1h20min for each membrane. During the filtration, TMP was controlled at 3±0.2bar and temperature was in the range between 26℃ and 32℃.

After collection, the feed and permeate samples were filtered with 0.45 µm filters MACHEREY-NAGEL GmbH & Co. KG and then stored in the fridge. Afterwards, the filtered samples were analyzed by a high performance liquid chromatography system (HPLC, Shimadzu, Japan), equipped with a size exclusive chromatography columns (SEC, 5 µm 30 Å, PSS Polymer Standards Service GmbH, Germany) and a refractive index detector (RID). The PEG that have different molecular weight show different elution time when passing through the columns, and its molecular weight corresponds to a specific elution time as displayed in the example of Figure 3.3. The signal triggered by PEG is proportional to the concentration of PEG in the samples.

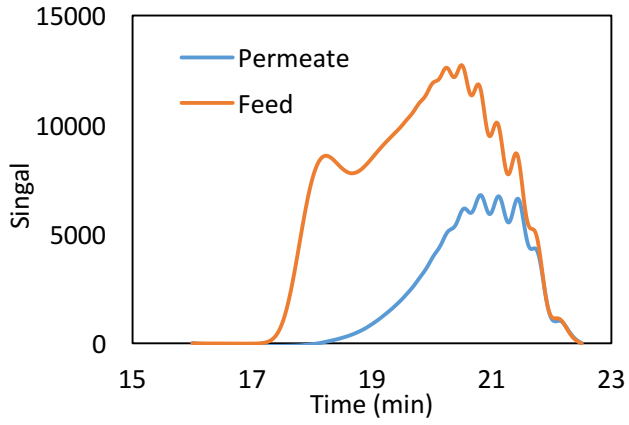

Figure 3.3 An example of signal curve of PEG samples

The PEG retention can be calculated by using Equation 3.3 :

$$R_i(\%) = \left(\frac{C_{i,feed} - C_{i,permeate}}{C_{i,feed}}\right) \qquad Eq.3.3$$

Where, $C_{i,feed}$ and $C_{i,permeate}$ are the PEG concentration in feed and permeate samples, respectively.

Figure 3.4 shows an accumulated rejection curve.

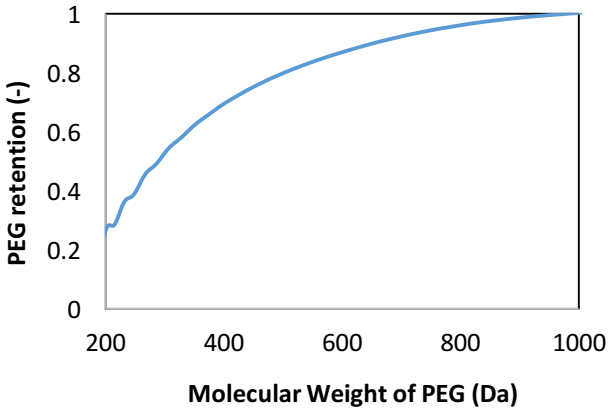

Figure 3.4 An example of retention curve

In addition, there is a correlation between the molecular size of PEG and their molecular weight, as shown in Equation 3.4 (Shang et al., 2017). Then, the pore size of the membrane could be calculated based on their MWCO, which is defined as the MW of the PEG that can be rejected by 90%.

$$d_s = 0.065\ (MW)^{0.437} \qquad Eq.3.4$$

Where d_s is the molecular diameter of PEG in nm; MW is the molecular weight of PEG in Da.

Calibration curve

The calibration curve, which was used to describe the relationship between elution time and molecular weight, is plotted by fitting a power model with elution time and molecular weight of standard samples. Figure 3.5 gives an example of calibration curve.

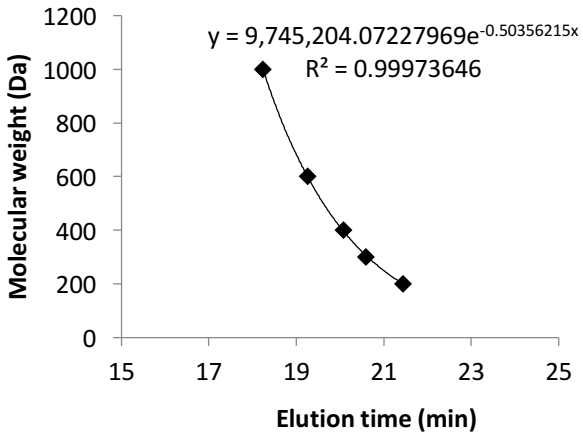

Figure 3.5 Calibration curve

3.4.3 Zeta-potential measurement

Zeta-potential measurement is performed on the membrane surface to investigate surface charge characteristic as a function of pH and ionic strength. The zeta-potential of pristine TiO_2 membranes was measured by an electrokinetic analyzer (SurPASS, Anton Paar, Graz, Austria) with a tangential mode. NaCl solutions with different ionic strength (Table 3.1) were used as background solution for zeta-potential measurements. The pH of the background solution was manually adjusted from from 4 to 8 (0.1M NaCl) and from 4 to 9 (0.01M NaCl). The zeta-potential measurements were performed under the temperature range between 22℃ and 25 ℃.

Table 3.1 Background solution for zeta-potential measurement

Electrolyte	Ionic strength (mol/L)	pH adjustment
NaCl	0.01	4~9
NaCl	0.1	4~8

3.5 Filtration experiments

3.5.1 Salt experiments

The feed solution for the salt filtration test was prepared by dissolving solid salts in ultrapure water. The solid salts sodium chloride (NaCl) and sodium sulphate (Na_2SO_4) were purchased from SIGMA-ALDRICH, Germany. During the salt filtration experiments, the feed solution was circulated through the membrane cell with a preset cross-flow velocity and operating pressure, which were adjusted by pump and valve. Different experimental conditions were applied for testing with various purposes, and they are summarized in Table 3.2.

The permeated samples were collected at 10 times intervals after 50 mins of stabilization. The feed samples were collected at the beginning and at the end time of the period of

permeate collection. The collected samples were filtered by 0.45 um filters (MACHEREY-NAGEL GmbH & Co. KG, Germany).

In the ionic strength experiment, the disk-shaped membranes were used for the low ionic strength conditions (0.01M and 0.1M) while the tubular membrane was used for the high ionic strength condition (1M). This is because the solution with high ion concentration has a higher osmotic pressure, and therefore requires a high operating pressure to keep the same permeate flux as in the low ionic strength condition.

Table 3.2 Summary of experimental conditions

Controlled Variable	Flux (LMH)	Crossflow velocity (m/s)	pH
pH	7±0.2	1.3±0.5	5±0.03 and 8±0.4
Ionic strength	7±0.2	1.3±0.5	8±0.4
Component	7±0.2	1.3±0.5	8±0.4
Cross flow velocity	14±0.5	1~7	8±0.4
Flux	15~75	1.3±0.1	8±0.3

3.5.2 Salt&NOM experiments

The NOM investigated in this study was humic NOM abstracted from the brine of anion exchangers in two drinking water treatment plants (PWNT, The Netherlands; Vitens N.V., The Netherlands). The feed solution was prepared by dissolving salt(s) and NOM into 2L demineralized water. The composition and preset ionic strength in the feed solution used in the different filtration experiments are summarized in Table 3.3.

Table 3.3 Composition of solution for Salt&NOM experiments

NOM -	Concentration of NOM g(DOC)/L	electrolyte -	Ionic strength mol/L
PWNT	0.5	NaCl	0.1; 1
		Na_2SO_4	0.1; 1
		NaCl+ Na_2SO_4	0.1; 1
Vitens	0.5	NaCl	0.1; 1
		Na_2SO_4	0.1
		NaCl+ Na_2SO_4	0.1; 1

For all of the salt&NOM filtration experiments, permeate flux was controlled at 30±2 $L/(h^{-1}m^{-2})$ and cross flow velocity was controlled at 1.3±0.04 m/s. The sampling started after 60min of filtration stabilization and the permeated samples were collected three times at an interval of 30min. Feed samples were collected when the first and the last permeated sample was taken. The collected samples were filtered through 0.45um glass fiber filters and stored in the fridge. The ultrapure water permeability was measured before each filtration test; the ultrapure water permeability tests were also repeated after each filtration test and forward flushing with 10-15 L of demiwater.

3.6 Analysis methods

3.6.1 Ionic chromatography

The concentration of Na^+, $SO4^{2-}$ and Cl^- in the feed and permeate water were determined by ionic chromatography (Metrohm Instruments, Swiss). Anions and cations can be identified based on their specific charge groups and interaction with an ion exchange column (Metrosep C6- 150/4.0, Metrohm Instruments, Swiss). The detecting range is 0.1-100 mg/L. Therefore, all the samples were diluted to the concentration within this range, preferably around 50 mg/L.

The observed ion rejection $\mathrm{R}(\%)$ was determined by Equation 3.4.

$$\mathrm{R}(\%) = \left(1 - \frac{C_p}{C_f}\right) \cdot 100 \qquad Eq.3.4$$

Where C_p and C_f are the solute concentration in the permeate and feed solutions, respectively.

3.6.2 Dissolved organic carbon

The Dissolved Organic Matters (DOC) in the feed and permeate samples was measured by a TOC analyzer (TOC-VCPH, Shimadzu Instruments).

3.6.3 Characterization of organic carbon

The liquid Chromatography-organic carbon detection (LC-OCD) was used to characterize organic matters in the original NOM solutions obtained from the water companies Vitens and PWNT. The LC-OCD method, performed by Het Waterlaboratorium (Het Waterlabotatorium N.V., The Netherlands), categorizes total organic matter into two groups, which are particular organic matters (POC) and dissolved organic matters (DOC); DOC is further categorized into 6 fractions: Biopolymers, humic substances (HS), building blocks, Neutrals, and Low Molecular weight acid and hydrophobic organic carbon. Each fraction was characterized based on their charge and size (Huber et al., 2011).

4 Membrane filtration: results and discussion

4.1 Membrane characterization

4.1.1 Water permeability and MWCO

Table 4.1 Water permeability and MWCO of the dish-shaped membranes (U01, U02 and U10) and a tubular membrane (T3). The SD is from triplicate measurements.

Membrane	Water permeability ($L\ h^{-1}\ m^{-2}\ bar^{-1}$)	MWCO (Da)
U01	8.26±0.47	518±12
U02	8.68±0.18	497±3
U10	14.28±0.12	464±4
T3	13.33±0.11	564±12

The membrane water permeability and MWCO of each membrane are shown in Table 4.1. All of the investigated membranes had MWCO approaching to 500Da and their water permeability varied from 8 to 13 L h^{-1} m^{-2} bar^{-1}. For comparison, the water permeability of ~500Da ceramic membranes is between 20 and 26 L h^{-1} m^{-2} bar^{-1}, as reported in other works (Weber et al, 2003; Puhlfürß et al., 2000; Shang et al., 2017). The membranes used in this case are less permeable than other ceramic membranes, probably because our membranes have a higher thickness or smaller porosity.

The disk-shaped membranes were used in the salt experiments while the tubular membrane was used in the salt&NOM experiments. As the three disk-shaped membranes have similar MWCO of ~500Da, they are referred as 500Da membranes in the following discussion. The tubular membrane, which has MWCO of 564Da, is further referred as 560Da membrane.

4.1.2 Membrane surface charge

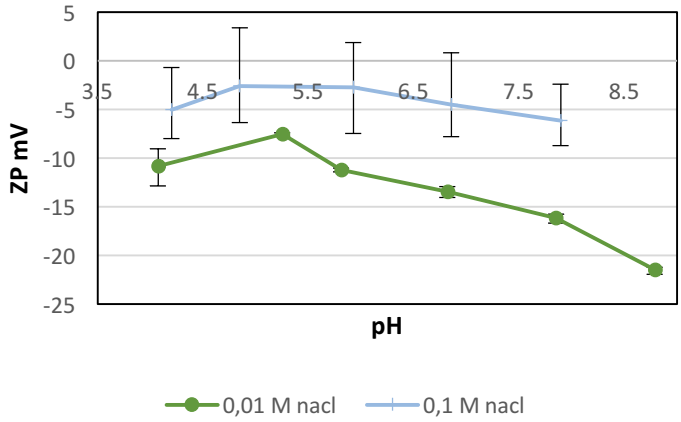

Figure 4.1 Zeta-potential as a function of PH of membrane immersed in NaCl electrolyte solution with ionic strength of 0.1M and 0.01M. Error bars show the standard deviation (SD) from duplicate measurements.

As shown in Figure 4.1, zeta potential of the measured ceramic NF membrane is negative with pH range from 5 to 9, which means that the membrane was negatively charged. Moreover, the zeta potential is pH-depended. Increase of pH shows an increasing in the magnitude of the zeta potential, which is due to the amphoteric nature of -Ti-OH surface groups (Van Gestel et al., 2002):

$$-Ti-OH+H_3O^+ = -Ti-OH_2^+ + H_2O \qquad (PH<6)$$
$$-Ti-OH+OH^+ = -Ti-O^- + H_2O \qquad (PH>6)$$

The zeta-potential of the measured membrane was lower for the 0.1M NaCl solution than in the 0.01M NaCl solution (Figure 4.1). This phenomenon can be attributed to the charge shielding effect and thus the suppression of the diffuse double layer. When ionic strength increases, a larger number of counter-ions shield the charge on the membrane surface, which causes a decrease of potential at the slipping plane (zeta potential) (Skluzacek et al., 2007). The specific adsorption of salt on the membrane surface can also alter surface charge (Tu, 2013). However, in this case, the contribution of ions adsorption to the surface with decreasing charge can be neglected, as there was no specific adsorption Na^+ and Cl^- ions on the ceramic membranes (Mullet et al., 1997; Zhao et al, 2005).

4.2 Salt experiments

4.2.1 Effect of pH on SO_4^{2-} rejection and Cl^- rejection

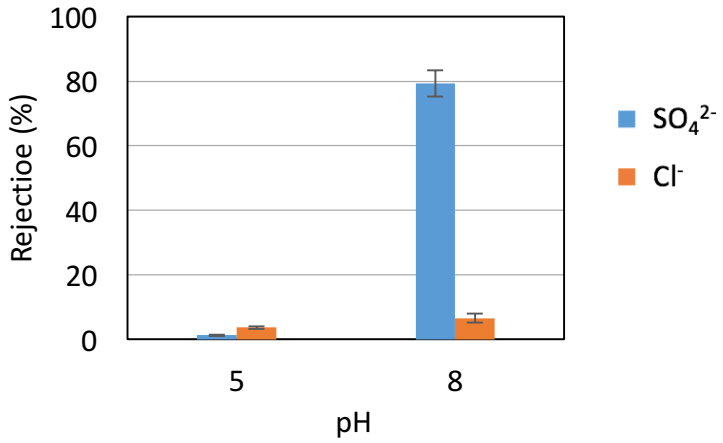

Figure 4.2 Rejection of SO_4^{2-} and Cl^- in the single salt solution at different pH. The ionic strength of salt in both feed solution is 0.01M. Error bars show the SD of parallel experiments done by three 500Da membranes.

Figure 4.2 shows that pH has a great impact on the separation of SO_4^{2-} and Cl^-. At pH 5, both anions were barely rejected (<5%) by the 500Da membranes. At pH8, the rejection of SO_4^{2-} increased greatly to 78.0%; the rejection of Cl^- also increased, but it was still minor, 2.9%. This can be explained by the zeta potential results.

At pH 5, the membrane showed almost no charge (Figure 4.1) and was thus unable to reject co-ions (SO_4^{2-} and Cl^-) by electrostatic repulsion. Under this condition, the rejection of SO_4^{2-}

and Cl^-) relied on size exclusion. However, since the hydrated diameter of ions (0.54nm of Cl^- and 0.60nm of SO_4^{2-}) (Tanganov, 2013) is smaller than the pore diameter of a 500Da membranes (0.989 nm), steric hindrance is not expected for both of these ions. As a consequence, the 500Da membranes showed no selectivity to SO_4^{2-} and Cl^- at low pH conditions due to the absence of charge effect and sieving effect. Other works report similar results: the selectivity of SO_4^{2-} and Cl^- could not be achieved by NF membranes near IEP were also reported in other works (Schaep et al., 1999; Szoke et al, 2003)

At pH8, the increased rejection of ions is due to the stronger charge effect. At high pH conditions, the membrane showed more negative charge (Figure 4.1), which indicates a stronger electrostatic repulsion. As the electrostatic repulsion increases, it is more difficult for the co-ions to enter into the membrane pores. Therefore, they are retained more on the feed side. The effect of the increased pH on rejection of SO_4^{2-} and Cl^- is different: at pH8, the SO_4^{2-} rejection was much higher than Cl^- rejection by the 500Da membranes. This can be explained by electrical interaction between charged ions and the charged membrane together with the mass transfer of ions. Due to its higher negative charge, SO_4^{2-} (divalent ion) has higher charge density than Cl^- (monovalent ion), and was therefore more electrostatically repelled by the charged membrane. Another factor might have also contributed to the higher SO_4^{2-} rejection: ceramic membranes appear to have more negative charge in a Na_2SO_4 solution than in a NaCl solution (Van Gestal et al., 2002), as a result of specific adsorption of SO_4^{2-} on TiO_2 surface (Kazarinov et al., 1981; Horányi, D., 2003). Moreover, diffusion predominates the mass transfer of monovalent ions in NF (Kelewou et al., 2011), and the diffusion coefficient of Cl^- is higher than that of SO_4^{2-} (Table 4.2). This facilitates the transport of Cl^- to the permeate side and leads to a low Cl^- rejection.

The results show that the rejection of SO_4^{2-} and Cl^- by 500Da membranes was considerably influenced by charge conditions of the ions themselves and of the membrane, whereas the rejection by sieving effect could be neglected.

Table 4.2 Diffusion coefficient of Cl^- and SO_4^{2-} at 25℃ (Meihong et al., 2008)

Anions	Diffusion coefficient , $\times 10^{-10}\ m^2 s^{-1}$
SO_4^{2-}	10.6
Cl^-	20.3

4.2.2 Effect of solution composition on SO_4^{2-} rejection and Cl^- rejection

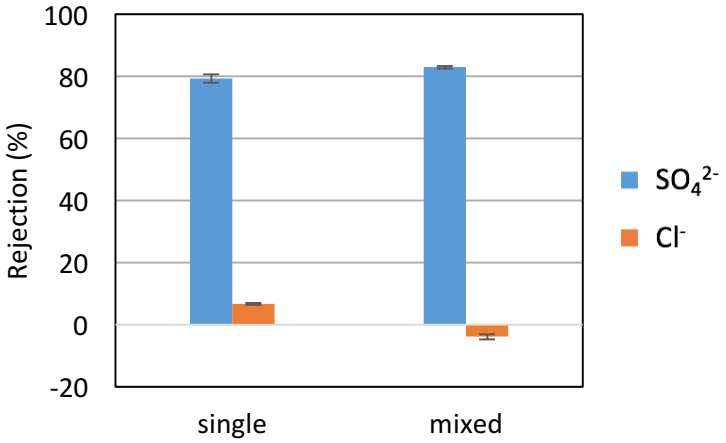

Figure 4.3 Rejection of SO_4^{2-} and Cl^- in single salt solution and mixed salts solutions at PH8. Single and mixed salt solution had the same ionic strength of 0.01M. Error bars show the SD of parallel experiments done by three 500Da membranes.

The rejection of SO_4^{2-} and Cl^- by 500Da membranes was investigated in solutions with different salt composition. The ratio of ionic strength between NaCl and Na_2SO_4 was 1:1 in the mixed solution to keep the same contribution of ions to the electrical double layer. Figure 4.3 shows that the retention of SO_4^{2-} improved slightly in the mixed solution when compared to the single solution. At the same time, the retention of Cl^-, already low in the single solution, decreased further and became negative in the mixed solution.

The rejection of Cl^- was 6.62±0.30 % in the NaCl solution while it was -3.96±0.76% in the mixed solution. The negative rejection of Cl^- can be explained by the Donnan distribution of salt between solution and membrane (Perry and Linder, 1989). In the mixed solution, the proportion of sodium is higher than in the single salt solution. As the membrane was negatively charged, cations (Na^+) were attracted by electrostatic force and tended to pass through the membrane, leading to the excess of positive charge in the permeate side. In order to keep the electro-neutrality, the monovalent anion (Cl^-) is dragged by Na^+ and transmit to the permeate solution, resulting in a negative retention. The negative rejection of Cl^- was always observed when NF membranes were applied to separate the mixed monovalent and multivalent ions (Tannins et al., 2006, Pere-Gonzalez et al., 2015; Gilron et al., 2001; Hagmeyer and Gimbel, 1999). The higher permeation of Cl^- in the mixed solution hindered the permeation of SO_4^{2-} which slightly enhanced the SO_4^{2-} rejection, as shown in Figure 4.3. However, the phenomenon that SO_4^{2-} rejection by NF membrane was not influenced by addition of Cl^- was previously observed by Déon et al.(2009). In addition, Krieg et al. (2004) reported that the in nanofiltration the SO_4^{2-} rejection was lower in a $NaCl/Na_2SO_4$ mixed solution where the ions ratio was 1:9, than in the pure solution, but no detailed explanation was given. The effect of Cl^- on SO_4^{2-} rejection in NF might need to be further investigated.

In mixed solutions, compared to single NaCl and Na_2SO_4 solutions, SO_4^{2-} was rejected more, and Cl^- was rejected less. However, the change of the two rejections was small. It suggests that solution composition played a minor role in the SO_4^{2-} and Cl^- separation by the 500Da membrane at experiment conditions applied in this study.

4.2.3 Effect of flux on SO_4^{2-} rejection

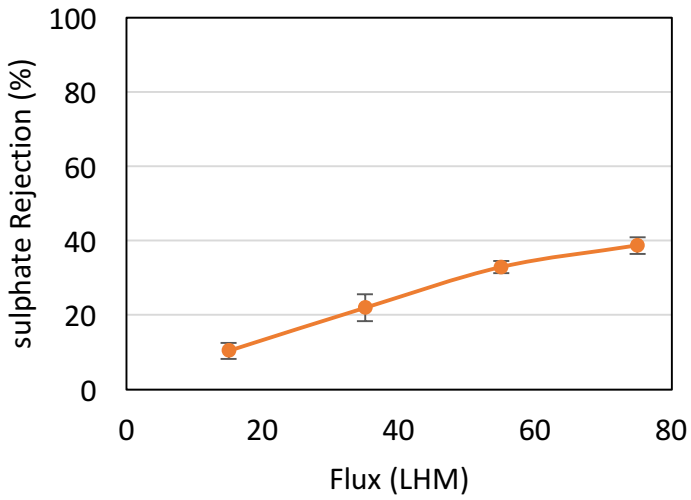

Figure 4.4 SO_4^{2-} rejection by ceramic NF membranes as a function of flux at PH 8. Error bars show the SD from duplicate experiments.

As illustrated in the Figure 4.4, when the permeate flux increased, the SO_4^{2-} rejection was higher. The rejection of SO_4^{2-} increased from 10.37% to 38.72 % when permeate flux increased from 15 LMH to 75 LMH. The flux increase was obtained by increasing the TMP.

When the TMP increases, the solvent flux increases proportionally, while the solute flux follows a diffusion process thus is not influenced by flux (Fang and Deng, 2014). The uncoupled behaviour of solvent flux and solute flux causes 'dilution effect'. Here was thus a lower concentration of solute in the permeate water, and consequently the solute rejection percentage increased.

4.2.4 Effect of cross flow on SO_4^{2-} rejection

SO_4^{2-} rejection was investigated at different cross flow velocities, ranging from 1 m/s to 7m/s. Figure 4.5 shows that the SO_4^{2-} rejection remained almost constant (about 20%) regardless of the increasing cross flow velocity. This result can be attributed to the turbulent flow (Re>3000) that occurred through all the experiments with different cross flow velocities (Table 4.3).

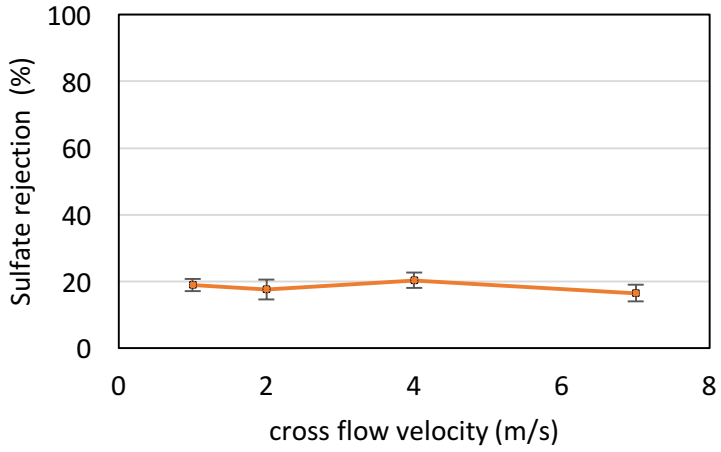

Figure 4.5 SO_4^{2-} rejection as a function of cross flow velocity. The ionic strength and PH in the feed solution is 0.1M and 8, respectively. Error bars show the SD from parallel experiments using two 500Da membranes.

During the filtration, a stagnant gel layer can be formed near membrane surface as a consequence of concentration polarization; the layer is effected by flow conditions (Déon et al., 2013). In case of high turbulence, the stagnant layer could have been minimized and, not affect the salt rejection.

Table 4.3 Reynolds number at different cross flow velocity. The Reynolds number was calculated based on the cross flow velocity near membrane surface and the hydraulic diameter estimated from the cross section of flow

Cross flow velocity (m/s)	Reynolds number
1	3572
2	7145
4	14290
7	25008

4.2.5 Effect of ionic strength on SO_4^{2-} rejection

The effect of ionic strength on sulphate rejection by 500Da membranes was investigated in the single Na_2SO_4 solution. The SO_4^{2-} rejection decreased with increasing ionic strength, which can be explained by the change of double layer inside the membrane pores. When ionic strength was low, the pore radius in NF membranes was small enough to form a double layer overlap in the pores, which contributed to co-ions repulsion. However, if ionic strength in the electrolyte solution was high, there was less double layer overlapping inside the membrane pores (Shang, 2014). With less double layer overlap, electrostatic interaction between the membrane and co-ions, $SO4^{2-}$ in our case, became weak. In addition, the effective area of membrane pores might have become larger due to the thinner double layer, which facilitates salt permeating (Wang et al., 2005; Yan et al., 2016). As a consequence, the effect of both charge and sieving in ions rejection became smaller when ionic strength is high, leading to a substantial decrease in SO_4^{2-} rejection.

The role of ionic strength and pore radius in retention performance can be quantified by Debye ratio. Debye ratio is the ratio of Debye length and pore radius. Debye length indicates the thickness of double layer and is inversely related to ionic strength, while Debye ratio represents the degree of electrical potential overlap (Shang, 2014).

$$k^{-1} = \left(\frac{\varepsilon_o \cdot \varepsilon_r \cdot K_B \cdot T}{2000 \cdot N_A \cdot e^2 \cdot I}\right)^{1/2} \qquad \text{Eq. 2.1}$$

$$\mathrm{I} = \frac{1}{2} \sum m_i \times Z_i^2$$

Where ε_o is vacuum permittivity in $CV^{-1}m^{-1}$ (8.85×10^{-12}); ε_r is relative permittivity of the background solution (80 for water at 20℃) ; K_B is Boltzmann constant (1.38×10^{-23}); T is absolute temperature in K; N_A is Avofadro number in mol^{-1} (6.0×10^{23}), e is elementary charge in C (1.6×10^{-19}); I is ionic strength in mol/L, m_i is molality of ion in mol/L; Z_i is charge number of ion.

The Debye length and Debye ratio in Table 4.4 were calculated by Equation 2.1. For the 500Da membranes, the increase of ionic strength that is from 0.01M to 0.1M led to a sharp decrease of Debye ratio that is from 5.22 to 1.65. Correspondingly, a considerable decrease in SO_4^{2-} rejection (from 79.33% to 18.37%) was observed. When the ionic strength further increased to 1M, the Debye ratio decreased slightly, and the SO_4^{2-} rejection only decreased by 10%. This result suggests that Debye ratio could be potentially used to estimate the rejection performance of the membranes based on their pore size and ionic strength in the solution.

Table 4.4 SO_4^{2-} rejection at different ionic strength of Na_2SO_4 at pH8. The SD of SO_4^{2-} rejection was from triplicate measurements. The ionic strength in the feed solution was measured by IC and the SD was from duplicate measurements.

Measured ionic strength (M)	Debye length (nm)	Debye ratio	SO42- rejection (%)
0.014±0.00	2.58	5.22	79.32±4.13
0.14±0.00	0.82	1.65	18.37±1.66
1.19±0.01	0.28	0.54	8.7±2.45

4.3 Salt&NOM experiments

4.3.1 NOM characterisation

Table 4.5 Organic composition of the NOM PWNT and the NOM Vitens

MW (Da)		~1000	300~500	<350
Proportion (%)	TOC	Humic substance	Building Blocks	Low molecular weight Neutrals
PWNT	100	85.6	12.5	6
Vitens	100	90.2	6.9	4.6

NOM was characterized by LC-OCD (Table 4.5). The LC-OCD confirms the humic nature of the NOM from PWNT and Vitens: Humic substance (HS), having MW of ~1000Da, were the main NOM fraction in both cases (85.6% for PWNT and 90.2% for Vitens). It is because humic acid are negatively charged compounds, therefore they are removed by anion-exchanger and are concentrated in the spent regenerant after regeneration of IEX-resin. Building blocks that is referred to the humic materials with lower molecular weight (Huber et al., 2011) were less (12.5% for PWNT and 6.9% for Vitens). A minor fraction of neutrals (6% for PWNT and 4.6% for Vitens) was detected as well. However, the neutrals were not expected to occur in the waste brine, as they are uncharged and therefore doesn't adsorb to the IEX-resin. The minor fraction of neutrals found in our case might be attributed to the instrument defects or measuring errors.

4.3.2 Rejection of NOM

Table 4.6 Rejection of NOM PWNT and NOM Vitens in the solutions with different composition and ionic strength. The ionic strength in the feed solution was measured by IC and the SD was from duplicate measurements. The measured concentration of NOM in feed solution was 0.5±0.3 DOCg/L.

Composition of feed water	Measured Ionic strength	Rejection of NOM (Vitens)	Rejection of NOM (PWNT)
	mol/L	%	%
NOM+Na_2SO_4	0.08±0.003	97.4±0.00	97.5±0.08
	0.7±0.004	-	96.6±0.04
NOM+NaCl	0.087±0.006	98.0±0.00	97.6±0.06
	0.79±0.01	97.6±0.00	94.1±0.10
NOM+ Na_2SO_4+NaCl	0.06±0.02	98.2±0.00	98.5±0.02
	0.89±0.07	97.6±0.00	97.0±0.09

As shown in Table 4.6, the 560Da membrane rejected more than 95% of both NOM from PWNT and from Vitens. Moreover, NOM rejection was unaffected by the variations of the ionic strength and composition of the solutions. This indicates that NOM removal by 560Da was independent of membrane charge, considering that membrane surface charge alters by

ionic strength. Therefore, the results suggest that the removal of NOM was due to the size exclusion.

Rejection of each NOM fraction can be explained by comparing their size (molecular weight) to the pore size of the membrane. PEG rejection is considered to be a representative for pore size distribution of the membrane. Figure 4.7 shows the PEG rejection curve of the 560Da membrane used in the NOM experiment. The membrane exhibited 90% rejection of components larger than 560Da, meaning that the humic substances (~1000Da) can be mostly rejected. Assuming that the building blocks have a MW of 400Da (average of 300Da and 500Da), we expected rejection of this fraction by approximately 70 %. For fraction smaller than 350Da, low molecular weight neutrals in our case, we expect a rejection lower than 40%; this indicates that the neutrals in the NOM could hardly be removed. Therefore, the expected rejection of NOM based on pore size distribution can be calculated by accumulating the rejection of humic substances and building blocks. As an example, the expected rejection of NOM of PWNT was 94.35%, which is the sum of 85.6% (100% removal of humic substances) and 8.75% (70% removal of building blocks). The expected rejection is in good agreement with the measured rejection shown in the Table 4.4, suggesting the importance of steric exclusion in the rejection of the NOM by the 560Da membrane.

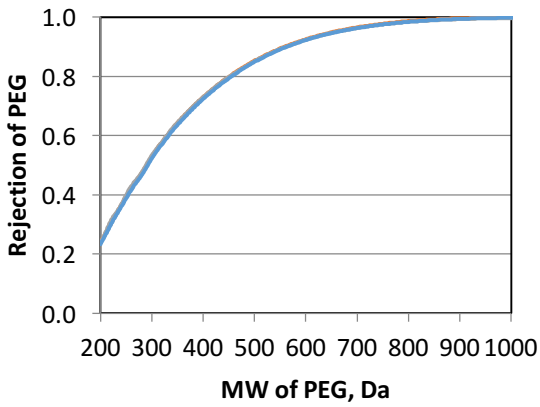

Figure 4.6 Rejection curve of the 560Da membrane from MWCO measurement

4.3.3 Effect of NOM on salts rejection

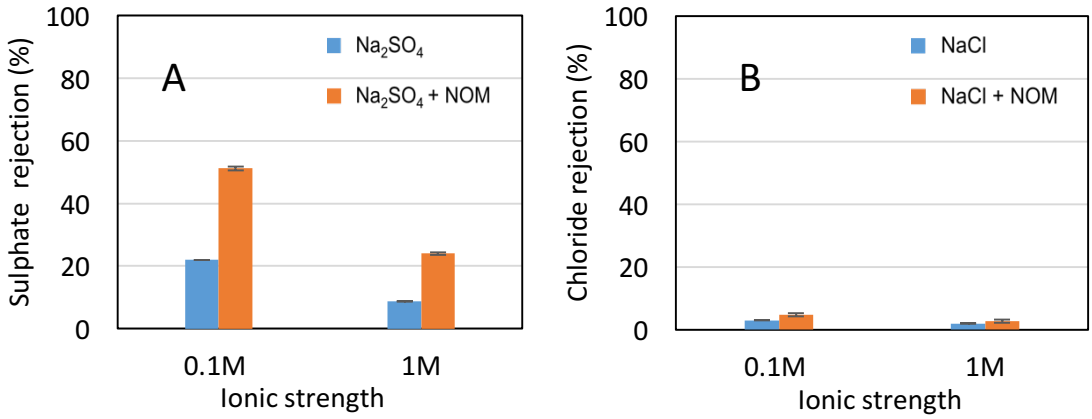

Figure 4.7 SO_4^{2-} rejection (A) and Cl^- rejection (B) at different ionic strength with the presence/absence of NOM PWNT. The error bars show the SD from duplicate measurements

As shown in Figure 4.7 (A), SO_4^{2-} rejection was between two and three times higher in solution with NOM than in the solution without NOM. However, when the ionic strength was high (1M), the 560Da membrane showed low rejection values for SO_4^{2-}, which is due to the less surface charge.

The improved SO_4^{2-} rejection might be explained by the stronger charge effect in the presence of NOM. Humic substances represent the largest fraction of the NOM tested in this study. They are negatively charged, because they contain abundant carboxylic groups and phenolic groups (Al-Amoudi, 2010). The functional group of humic substances and the hydroxide groups on the TiO_2 membrane surface tend to be hydrogen bonded with each other (Mustafa et al., 2016). As a result, the membrane surface charge can be influenced by the surrounding humic substance. De Lara and Benavente (2009) reported that ceramic membranes fouled with protein had a greater negative surface charge than non fouled membranes. In addition, it is also possible that the charged NOM accumulate in the polarization layer, which could enhance the charge effect and increases the SO_4^{2-} rejection substantially (Wesselingh and Krishna, 2000).

A second hypothesis for the improved SO_4^{2-} rejection is the pore constriction that might be caused by NOM. Shang et al. (2015) concluded that small organics might attach to the inner pores of the membrane, narrowing the effective pore size and increasing the steric hindrance. The enhanced retention performance of NOM-fouled NF membranes due to the higher steric hindrance was also observed by Nghiem et al. (2009). However, an experimental study of the characteristics of NOM and its effect on the salt rejection by ceramic NF membranes is still required.

For Cl^-, the rejection was less than 5% though it showed a slight increase with the addition of NOM to the solution (Figure 4.7 (B)). The complete permeation of Cl^- was probably a combination of their low charge density and high mobility, as explained in Section 4.2.1.

4.3.4 Concentration polarization in salt&NOM experiments

The concentration polarization (CP) factor (β) was used to reflect the extent of concentration polarization close to the membrane surface during filtration. It can be calculated based on the mass transfer of solutes on the feed side, the hydraulic conditions during the experiments and the geometry of the membrane system (Verberk, 2005). The CP factor (β) can be expressed as Equation 4.1.

$$\exp\left(\frac{J \cdot \delta}{D}\right) = \beta \qquad Eq.4.1$$

where J is the flux in $m^3/(m^2 \cdot s)$, D is the diffusion coefficient in m^2/s , δ is the thickness of the laminar boundary layer in m.

The ratio of the laminar boundary layer and the diffusion coefficient is called mass transfer coefficient (k). It can be expressed in an empirical Sherwood relationship where the Reynolds number (Re), Schmidt number (Sc) and geometry parameters of the membrane are introduced, as shown from Equation 4.2 to Equation 4.5 (Verberk, 2005).

$$\mathrm{k} = \frac{D}{\delta} \qquad Eq.4.2$$

$$\mathrm{Sh} = \frac{k \cdot d_n}{D} \qquad Eq.4.3$$

$$\mathrm{Re} = \frac{u \cdot d_n}{v} \qquad Eq.4.4$$

$$\mathrm{Sc} = \frac{v}{D} \qquad Eq.4.5$$

Where Sh is the Sherwood number; d_n is the hydraulic diameter (in this case, the inner diameter of membrane) in m; u is the characteristic velocity in m/s, v is the kinematic viscosity in m^2/s.

The empirical Sherwood relationship has different expressions depending on membrane configurations and fluid motions. For tubular membranes performed in turbulent flow, the Sherwood relationship was available in literature (Linton and Sherwood, 1950).

$$\mathrm{Sh} = 0.04 \cdot Re^{\frac{3}{4}} \cdot Sc^{\frac{1}{3}} \qquad Eq.4.6$$

It should be noted that both salt and NOM can contribute to concentration polarization in NF (Winter et al., 2017). However, CP caused by NOM can not be calculated by the Sherwood model because the diffusion coefficient of NOM is unavailable in literatures. It leaves some space for the study of diffusivity and other mass transfer mechanisms of NOM during NF. Here, the calculated CP factor only represented the extent of CP caused by ions near the membrane surface.

The fixed parameters and assumptions for polarization factor calculation are listed as following.

1. The hydraulic diameter is the inner diameter of the tubular membrane that was 0.007m;

2. Characteristic velocity is cross flow velocity, which was 1.3 m/s;

3. Kinematic viscosity of Na_2SO_4 solutions and NaCl solutions at the applied temperature

and ionic strength were found in literatures (Kestin et al., 1981; Abdulagatov et al., 2005);

4. Diffusion coefficient of Na_2SO_4 and NaCl with the applied ionic strength were found from literatures (Poupeleer et al., 2003; Vitagliano and Lyons, 1956)

5. The flux was measured in the experiments.

Table 4.7 CP factors in NOM (PWNT) experiments for different solution composition and ionic strength

Composition of feed solution	ionic strength	kinematic viscosity	diffusion coefficient	CP factor
	M	×10-7 m^2/s	×10-10 m^2/s	-
NOM+NaCl	0.1	8.01	14.9	1.113
NOM+NaCl	1	8.13	15.1	1.122
NOM+Na_2SO_4	0.1	8.15	9.80	1.156
NOM+ Na_2SO_4	1	7.80	6.65	1.216

As shown in Table 4.7, the CP factor approached to 1 in all experiments which means that almost no concentration polarization occurred near the membrane surface due to the accumulation of ions.

4.4 Necessity of membrane modification

In this study, the 500Da NF membranes were able to separate SO_4^{2-} and $Cl^-$when the membrane surface was negatively charged: the divalent SO_4^{2-} has a higher negative charge, and was thus more rejected by charge than the monovalent Cl^-, which permeated through the membrane. However, the charge effect didn't occur at high ionic strength due to less double layer overlapping in the pores; these facilitated anions to go through the membrane, and causes a low rejection of SO_4^{2-} and a impure NaCl permeate. Without charge effect, the separation of ions relied on sieving effect. Therefore, our approach will focus on pore size reduction to achieve a separation of SO_4^{2-} and Cl^- at high ionic strength.

4.5 Suggestions of the desired pore size

The hydrated radius of SO_4^{2-} (0.3nm) is only slightly higher than that of Cl^- (0.27nm) (Tanganov et al., 2013). However, compared to Cl^-, SO_4^{2-} has a higher hydration free energy, which helps itself to hold the hydration shell (Tansel, 2012). In contrast, the hydration shell of Cl^- is easy to break and the hydrated radius of Cl^- will become smaller when passing through the membrane pores. As the difference of hydrated size of two ions will become greater in the membrane pores, it should be possible to separate them. The desired pore radius of the membrane should be closed to the hydrated radius of SO_4^{2-} in order to reject SO_4^{2-} only. Converting the pore radius to the MWCO by using the Equation 3.4 in the Section 3.4.2, the aim MWCO of the membrane should be around 300Da.

5 Membrane modification: materials and methods

5.1 Substrate membranes

Commercial disk Ceramic NF membranes were used as substrate membranes for ALD coating. Their characteristics have been described in the Section 3.1. The MWCO of these membranes were claimed as 450Da according to the supplier, but a much higher MWCO was observed in this study. Therefore, we determined the MWCO of the membranes using the PEG rejection experiments, as described in Section 3.4.2.

5.2 Atomic Layer Deposition

The high-vacuum ALD system (Fiji®, Vecco, the Netherlands) was used to coat TiO_2 on the ceramic membrane. Titanium tetrachloride ($TiCl_4$) and water vapour (H_2O) were used as precursors. At the beginning of the ALD process, $TiCl_4$ was pulsed to the ceramic substrate and chemically reacted with surface groups, generating abundant surface site as well as by-products. After the pulse, the residual $TiCl_4$ and by-products were purged by inert gas. Then, H_2O was pulsed and reacted with surface sites to finish one coating cycle. As the binary surface reactions occurred sequentially, TiO_2 was deposited on the substrates. The two surface reactions can be described as (Shang et al., 2017):

$$n(-OH)^* + TiCl_4(g) \rightarrow (-O-)_n(TiCl)_{4-n}{}^* + nCH_4\,(g) \quad (A)$$

$$(-O-)_n(TiCl)_{4-n}{}^* + H_2O(g) \rightarrow (-O-)_nTi(OH)^*_{4-n} + (4-n)HCl(g) \quad (B)$$

Where asterisks represent the surface species.

The ALD process was operated at a preset temperature of 180 ℃. The duration of pulse process and purge process was summarized in Table 5.1.

Table 5.1 Recipe of TiO_2 ALD for one coating cycle

Steps	time (s)
$TiCl_4$ pulse	0.2
Purge	11
H2O pulse	0.2
Purge	16

5.3 Membrane coating

The substrate membranes were firstly coated with several cycles, and, after a MWCO tests, they were coated a second time, with the aim to reach the desired MWCO (300Da). The coating cycles for each membrane were determined based on the desired MWCO reduction and the estimated thickness of a monolayer of TiO_2. The thickness of a monolayer of TiO_2 was estimated from pre-tests on silicon wafers by using the same recipe as used for membrane coating. The number of coating cycles for each membrane during the two ALD coatings is shown in Table 5.2. The coating cycles for each membrane could be different in the first ALD (1 ALD) and the second ALD (2 ALD), since they have different initial MWCO and need to be coated with different cycles to reach the aim MWCO (300Da).

Table 5.2 Coating cycles of substrate membranes in two ALD processes

Substrate membranes	1 ALD (Cycles)	2 ALD (Cycles)
F6	4	3
F11	5	5
F12	4	5
U15	5	4
U35	4	3
U38	3	3
U39	5	2
LY5	3	2
LY8	3	4

5.4 Thickness of TiO_2 on wafers

The Ellipsometer (M-2000F, J.A. Woollam Co. Inc., USA) was used to measure the thickness of the deposited TiO_2. The measurement relies on the change in polarized light reflected from the sample surface (Airaksinen et al., 2015). Since the membrane pores have a curved surface, the direct measurement of TiO_2 thickness inside membrane pores is not feasible. Therefore, silicon wafers with a flat surface were used to monitor the growth of the TiO_2 layer. When coating the substrate membrane, a silicon wafer (1.5cm× 1.5cm) was placed next to the membrane in the reactor chamber, and was coated as well. The measurement of thickness on the wafer surface was performed on 5 measuring points, as shown in Figure 5.1.

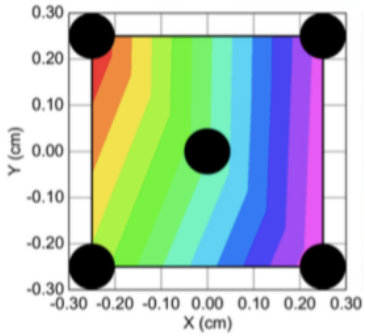

Figure 5.1 Five measuring points on the wafer surface

By measuring the thickness of the uncoated wafer and the coated wafer by Ellipsometer, the thickness of deposited TiO_2 layer can be calculated. The Growth per Cycle (GPC) of TiO_2 layer can therefore be calculated by dividing the coating thickness by coating cycles, as shown in Equation 5.1.

$$\mathrm{GPC} = \frac{d_2 - d_1}{A} \qquad Eq.5.1$$

Where d_2 and d_1 are the average thickness of the coated wafer and uncoated wafer in nm, respectively; A is Coating cycles

5.5 Characterization methods

5.5.1 Water permeability and MWCO

The water permeability and MWCO were measured on the pristine membranes and the coated membranes (both 1ALD and 2 ALD). The measuring methods and analysis methods have been described in the Section 3.4.

5.5.2 Defects

As the maximum MW of PEG used for the MWCO measurement in this study was 1000Da, the defects in this experiment was defined as the percentage of 1000Da PEG that was not totally rejected by the measured membrane.

6 Membrane modification: results and discussion

6.1 Growth per cycle of TiO_2

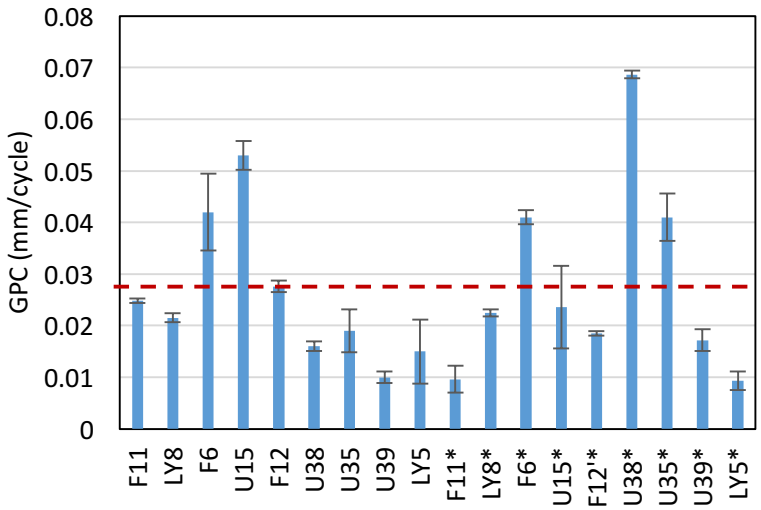

Figure 6.1 The GPC of TiO_2 on the wafer in the first coating (membrane without asterisks) and the second coating (membrane with asterisks). Error bars show the SD from 5 measuring points.

The GPC of TiO_2 on the wafer (the dot red line) is 0.027nm/cycle. However, a great deviation of GPC was observed in this study, which means that the coating processes was not stable.

Literature shows that the growth of TiO_2 is greatly influenced by operating temperature. At temperature below ~150 ℃, purging become less effective in removing physically adsorbed species, which remains on the substrate surface and reacts with the next precursor (Triani et al., 2006). These physically adsorbed species probably contribute to a higher growth rate (Triani et al., 2006). Therefore, the great deviation of GPC observed in this study might be caused by the inconstant temperature in the reactor chamber during the deposition, though the temperature was preset.

6.2 Membrane characterisation

The membrane characteristics including MWCO, water permeability and defects were measured before and after each of the two ALD coatings. These data can be found in table 6.1. After the first coating, the water permeability of the membranes decreased dramatically, and the MWCO of the membranes decreased correspondingly. The great loss of water permeability indicates the considerable influence of TiO_2 coating on membrane productivity. After the second coating, the water permeability further decreased, but the MWCO increases, contrary to our expectation. The defects of the membranes increased as the number of coating increased. In order to explain the increase of MWCO after the seconding coating, a theoretical analysis was performed with respect to the flux distribution and pore size distribution, using one membrane as an example.

Table 6.1 Water permeability, MWCO and defects of pristine membranes and coated membranes. The SD is from triplicate measurements

	MWCO(Da)			Water Permeability (L h-1 m-2 bar-1)			Defects (%)		
	pristine	1 ALD	2 ALD	pristine	1 ALD	2 ALD	pristine	1 ALD	2 ALD
F6	724±13.5	640±3.9	866±13.3	22.8±0.52	3.5±0.05	2.1±0.05	0.91	2.00	6.11
F11	883±43.3	793±9.2	1080±19.8	33.7±0.89	8.5±0.1	3.1±0.39	5.3	4.2	9.98
F12	810±14.0	720±15.9	1222±54.3	34.0±0.32	8.3±0.1	1.7±0.14	2.5	3	10.76
U15	754±16.0	652±5.7	786±28	34.7±0.21	11.8±0.17	10.4±0.29	2.3	2.7	3.2
U35	746±29.8	600±10.3	849±13.8	21.0±0.38	6.0±0.07	1.6±0.15	1	2.1	6.6
U38	726±19.9	638±11.4	994±24.0	22.6±0.26	5.3±0.2	1.5±0.25	0.9	3	9.66
U39	790±13.1	533±18.4	645±8.21	17.5±0.17	6.8±0.06	3.1±0.22	2.3	2	3.64
LY5	643±8.4	497±15.7	534±31.5	16.2±0.24	4.5±0.04	2.3±0.22	0	0	1.47
LY8	829±18.2	654±11.4	989±1.08	20.9±0.29	5.2±0.04	0.6±0.10	4.2	2.6	8.65

7 Membrane modification: theoretical analysis

7.1 Flux distribution

According to the Hagen-Poiseulle equation (Equation 7.1), the membrane flux increases with the pore size, if the TMP, the length of pore, the number of capillary and the viscosity of liquid are the same. Therefore, the membrane flux distribution can be used to study the contribution of different sized pores to the total flux. In this chapter we will show the flux distribution for the example membrane F6.

$$\mathrm{Q} = \frac{\pi \cdot r^4 \cdot \Delta P_T}{8 \cdot \mu \cdot L} \cdot m \qquad Eq.7.1$$

Where Q is flow rate in m3/s; r is pore radius in m, ΔP_T is TMP in Pa; μ is viscosity of liquid in pore in $Pa \cdot s$; L is the length of pore in m, m is the number of capillaries.

In the PEG filtration experiment, PEG molecules follow the water flux. The PEG rejected by the pores with a certain size has a correlation with the flux though the pores with the same size. Their correlation can be deduced by the following procedure, with the following assumptions:

1. The pore size is divided into 10 intervals: <200Da, 200Da-300Da, …, >1000Da.

2. PEG is rejected by sieving effect only. The effect of charge and diffusion on PEG rejection is not considered.

3. PEG can pass through the membrane pores that has the same size and larger size than PEG.

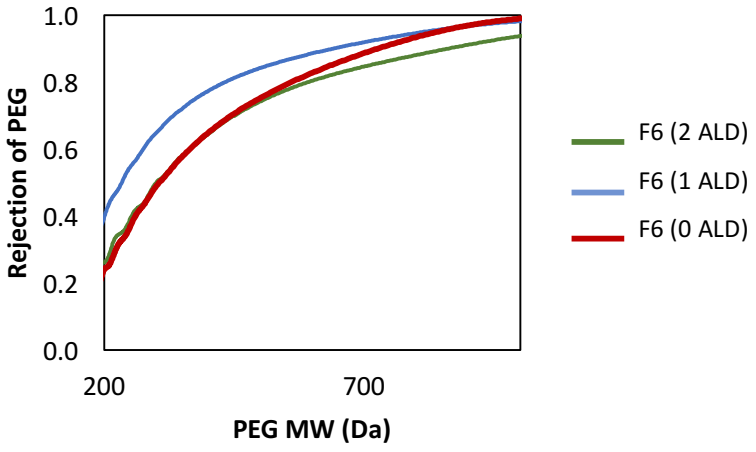

Figure 7.1 Rejection curve of membrane F6 before coating and after two times of coating

The correlation between flux and rejection of PEG was derived based on the definition of rejection. For example, the rejection of PEG within MW of 300Da (R_{300}) can be calculated as:

$$R_{300} = 1 - \frac{C_{300}}{C'_{300}} = \frac{\frac{F_{300} \cdot C'_{300} + F_{>300} \cdot C'_{300}}{F_T}}{C'_{300}} = 1 - \frac{F_{>300}}{F_T} \qquad Eq.7.2$$

$$F_T = F_{<200} + F_{200} + F_{300} \cdots\cdots + F_{1000} + F_{>1000} \qquad Eq.7.3$$

Where C_{300} and C'_{300} are the concentration of PEG with WM of 300 in the permeate solution and feed solution in g/L, respectively; F_T is the total flux in L h^{-1} m^{-2}.

The calculation was the same for rejection of PEG with MW of 400Da.

$$R_{400} = 1 - \frac{F_{>400}}{F_T} \qquad Eq.7.4$$

The difference of PEG rejection is the ratio of flux through a certain size of pore to the total flux. Then, the flux distribution can be calculated based on the flux measured in the PEG filtration experiment and the correlation between flux and PEG rejection:

$$R_{400} - R_{300} = \frac{F_{>300}}{F_T} - \frac{F_{>400}}{F_T} = \frac{F_{300-400}}{F_T} \qquad Eq.7.5$$

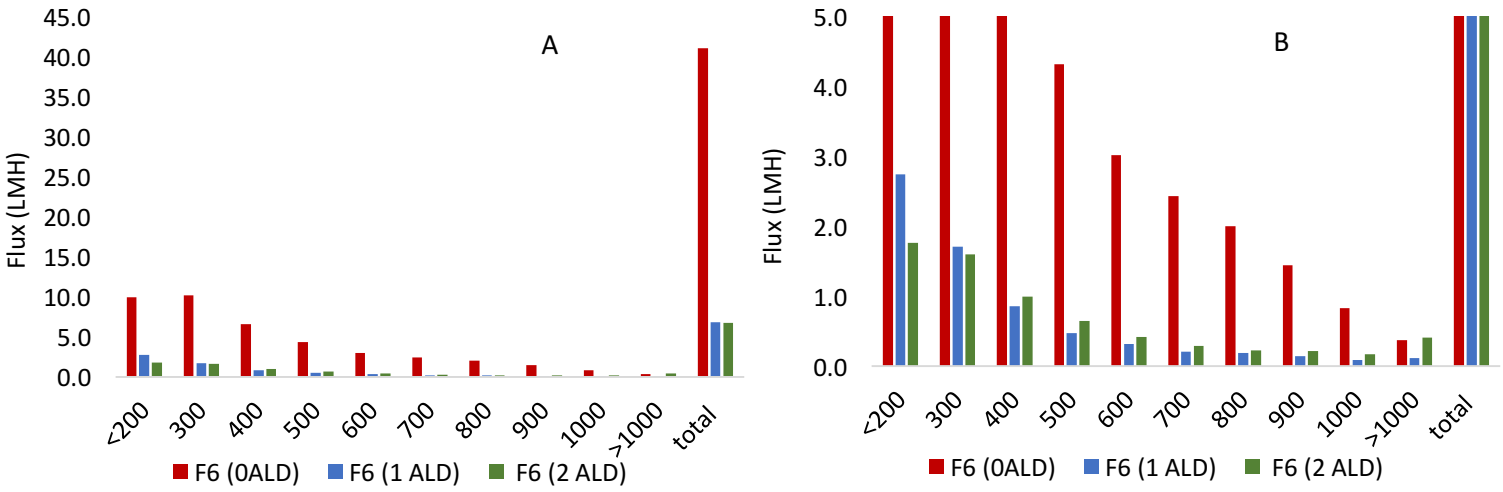

Figure 7.2 Flux distribution of membrane F6 before coating and after two times of coating (A: original Figure; B: Enlarged Figure)

Figure 7.2 shows that, after the first coating, the flux through all the pores decreased, meaning that the size of all the pores decreased due to the deposited TiO_2 layer. After the second coating, the flux through the pores less than 300Da (small pores) decreased whereas the flux through the pores higher than 400Da (big pores) increased. This suggests that some of the small pores were blocked during the second coating, and were not replaced by coated larger pores. Therefore, the flow tended to go through the large pores and defects, resulting in an increased flux contribution of large pores and defects. Under this

circumstance, the PEG will pass through the large pores and causes an increased MWCO as observed in the experiment.

The flux through defects also increased after the second coating. The defects allowed compounds larger than 1000Da to permeate through the membrane, which deteriorated the selectivity of the membrane and contributed most to the increase in MWCO. Thus, compared to the small pores, the defects and large pores are more important for flux and MWCO. The contribution of large pores and small pores can be demonstrated by Hagen-Poiseulle equation (Equation 7.1). If the total area of a certain number of small pores (m) and large pores (n) is the same, their radius is correlated:

$$A_b = A_s \qquad Eq.7.6$$

$$n \cdot \pi r_b^2 = m \cdot \pi r_s^2 \quad \longrightarrow \quad r_b = \sqrt{\frac{m}{n}} r_s \qquad Eq.7.7$$

Therefore, the flux in the pores is related to the pore size: :

$$\frac{Q_b}{Q_s} = \frac{A \cdot r_b^4}{A \cdot r_s^4} = (\frac{m}{n})^2 \qquad Eq.7.8$$

Where A is a combination of constant parameters which are TMP, the length of pore and the viscosity of liquid.

Consequently, the flux in large pore is higher than in small pores, even the large pores and small pores have the same area. This result confirms the importance of large pores and defects in the flux distribution.

7.2 Pore size distribution

The pore size distribution of pristine membranes and coated membranes were modelled to investigate the change of pore size during the deposition. Assuming that the pore size of the NF membranes follows log-normal distribution, the PEG rejection curve can be simulated by a log-normal model as a function of MW and MWCO, as described in Equation 7.9 (Shang et al., 2017).

$$\sigma(\mathrm{MW}_s) = \int_0^{\mathrm{MW}_s} \frac{1}{S_{MW}\sqrt{2\pi}} \frac{1}{MW} \exp\left[-\frac{(\ln(MW) - \ln(MWCO) + 0.56S_{MW})^2}{2S_{MW}^2}\right] \qquad Eq.7.9$$

where $\sigma(MW_s)$ is reflection coefficient, S_{MW} is standard deviation of molecular weight retention , MW is molecular weight.

Further, the pore size can be calculated based on the MW of the PEG molecules. Based on PEG/HPLC measurement and a log-normal model, the pore size distribution of the pristine membrane and the coated membrane is shown in Figure 7.3, of an example membrane F6.

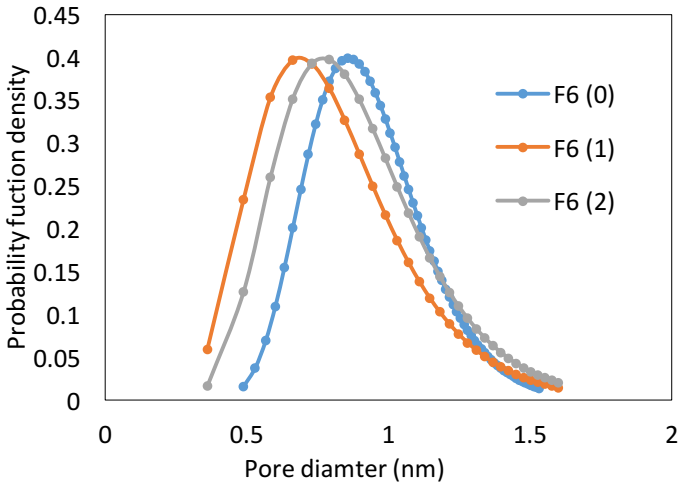

Figure 7.3 Modelled pore size distribution of pristine membrane F6 and the coated membrane F6 with 1ALD and 2 ALD

After the first coating, pore size reduction was observed among all the pores. However, the extent of the decrease was different between small pores (pore diameter less than 0.9nm) and large pores (pore diameter higher than 0.9nm). This is due to the fact that one deposited layer has greater contribution to the deceasing of area in the small pores than in the large pores. After the second coating, the small pores disappeared due to the pore blocking, and thus all the PEGs in the permeate passed through the large pores, as explained in Section 7.1. This behavior is reflected as the shift of distribution curve after the second coating (from orange line to grey line), as shown in Figure 7.3.

In the study of Shang et al. (2017), when TiO_2 was deposited on the TiO_2-based ceramic membranes by the approach of APALD, the effect of coating on the large pores and small pores in the pristine membrane was different from that observed in this study. Figure 7.4 shows the pore size distribution of both pristine and APALD-coated membrane, by using the calculations methods described above. After coating, the reduction of pore size of large pores was large than the reduction of the small pores, which also led to a narrow pore size distribution. Comparing the results from vacuum ALD and APADL, it can be concluded that APALD was effective in decreasing the size of relatively large pores, while the vacuum ALD affects the size of relatively small pores greatly. However, the reasons for this phenomenon need to be further studied.

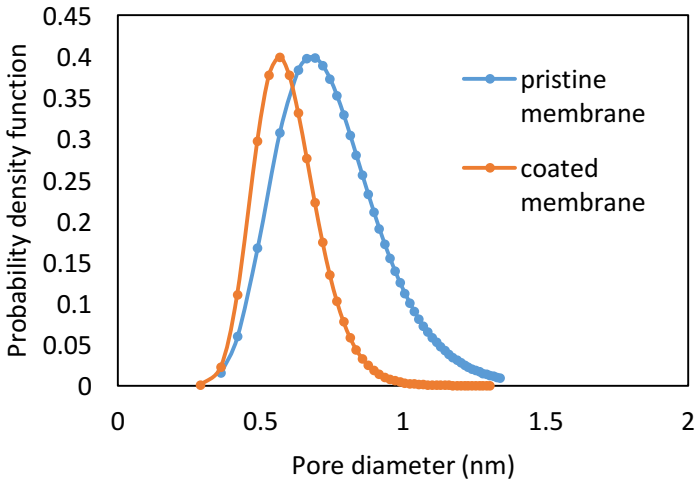

Figure 7.4 Modelled pore size distribution of the pristine membrane and the coated membrane (Data source: Shang et al., 2017)

8 Conclusions and recommendations

8.1 Conclusions for membrane filtration

The conclusions for membrane filtration are drawn based on the research questions:

- What is the effect of operational parameters on the rejection of NaCl and Na_2SO_4 ?

Salts experiments were carried out to investigate the effect of nature of solutions (i.e. pH, ionic strength, solute composition) and operating conditions (i.e. cross flow velocity, operating pressure) on the salts rejection by negatively charged 500Da NF membranes. The higher pH led to an increased rejection of anions, since the membranes have more negative charge at higher pH. The salt composition in the solution affected the rejection of SO_4^{2-} and Cl^- based on the Donnan effect. A slight increase of SO_4^{2-} rejection and a slight decrease of Cl^- rejection was observed in the mixed solution compared to that in the single salt solution. In the experiments mention above, the Cl^- rejection was always low (<5%), whereas the SO_4^{2-} rejection was relatively high (>80%). Therefore, only SO_4^{2-} rejection was investigated in the following experiments being subject to ionic strength, cross flow velocity and operating pressure.

The higher ionic strength led to a lower rejection of SO_4^{2-}, which was a result of compressed double layer inside membrane pores. The 500Da membranes yielded a low SO_4^{2-} rejection (11.85%) at ionic strength of 0.1M at pH 8. The cross flow velocity had no influence in the SO_4^{2-} rejection in the case of high turbulence. In addition, the incremental operating pressure resulted in the increase of SO_4^{2-} rejection, since the SO_4^{2-} was diluted in the permeate side at high operating pressure.

- What is the influence of NOM on rejection of highly concentrated salts (NaCl and Na_2SO_4) by ceramic NF membranes? And what is the influence of salts on NOM rejection?

Salt&NOM experiments were performed on a negatively charged 560Da NF membrane. The salt rejection increased after addition of NOM, possibly because the membrane was more negatively charged in the presence of NOM. However, a decrease of salt rejection was observed when the ionic strength was higher. The SO_4^{2-} rejection and Cl^- rejection were relatively low at high ionic strength conditions (1M), at 24% and 2.8% respectively, despite the presence of NOM.

The 560Da NF membrane exhibited a high rejection of NOM (>95%) due to the effective steric exclusion. Moreover, ionic strength of salts and solution composition had no effect on NOM rejection. It means that NOM rejection by 560Da NF membrane is independent of membrane surface charge.

- Can Salts (NaCl and Na_2SO_4) be separated from salts/NOM mixtures at high ionic strength?

In conclusion, the 560Da NF membrane is capable to separate NOM and salts from the mixtures at high ionic strength conditions.

8.2 Recommendations for membrane filtration

8.2.1 Improvement of salts&NOM experiment

The charge properties of NOM and the NOM-fouled membrane was not investigated in this study. However, the charge effect is important for salt rejection in NF. In the future studies, it is recommended to measure the charge of NOM and the NOM-fouled membranes, since it helps to understand the effect of NOM on the salt rejection.

8.3 Conclusions for membrane modification

In this study, commercial ceramic NF membranes with initial pore size between 600Da – 900Da were coated twice by vacuum TiO_2 ALD, in order to obtain a desired MWCO of ~300Da. The conclusion for membrane modification is drawn based on the research question:

- How can we modify the pore size of ceramic NF membranes by approach of vacuum TiO_2 ALD?

The average growth per cycle (GPC) of TiO_2 was 0.027nm/cycle, but there was a great deviation of the growth rate per cycle. A possible reason for it could be unstable temperature.

The analysis of flux distribution and pore size distribution of pristine membranes and coated membranes shows that the contribution of relatively small pores to the total flux decreased after the second coating, as a result of pore blockage. The blocked pores negatively influence the membrane performance, which was indicated by the increased MWCO. Furthermore, the effect of defects and large pores to the membrane selectivity became large when small pores were blocked.

Comparisons between the vacuum ALD and APALD shows that APALD was more effective in coating the relatively large pores than the relatively small pore in the NF membranes.

In conclusion, the modification of the ceramic NF membranes by vacuum TiO_2 ALD was not successful in our case.

8.4 Recommendations for membrane modification

Based on the experimental results from ALD and PEG rejection tests together with the theoretical analysis, the following recommendations are made:

1. The ALD processes might need to be optimized in terms of temperature control. It might be necessary to install a temperature controller to maintain a constant temperature in the ALD chamber. Also, the temperature of the substrate should be monitored during the ALD, to unsure that the substrate has the same temperature as the preset one.

2. Membranes with less defects are needed as substrate for the coating process, as defects are responsible for the low selectivity of membranes, especially when the membrane only has a small proportion of relatively small pores.

3. Substrate membranes with smaller initial MWCO, more close to the aimed MWCO, are recommended for coating. In that case, the fewer coating layers are needed, lowering the risk of pore blocking.

4. A detailed study about the comparison of vacuum ALD and APALD is suggested to be carried out to get a better insight of the differences between the two types of ALD and of the influence of atmospheric pressure on coating.

References

Abdulagatov, IM, Zeinalova, A., & Azizov, ND (2005). Viscosity of aqueous Na_2SO_4 solutions at temperatures from 298 to 573 and at pressures up to 40 MPa. *Fluid Phase Equilibria* , *227* (1), 57-70.

Ahmed, A. (2013). *Rejection and Critical Flux of Calcium Sulphate in a Ceramic Titanium Dioxide Nanofiltration Membrane* (Doctoral dissertation, The University of Manchester (United Kingdom).

Airaksinen, V. (2015). Handbook of Silicon Based MEMS Materials and Technologies (Second Edition)

Al-Amoudi, A. S. (2010). Factors affecting natural organic matter (NOM) and scaling fouling in NF membranes: a review. *Desalination*, *259*(1-3), 1-10.

Al-Zoubi, H., & Omar, W. (2009). Rejection of salt mixtures from high saline by nanofiltration membranes. *Korean Journal of Chemical Engineering*, *26*(3), 799-805.

Amin, S. K., Abdallah, H. A. M., Roushdy, M. H., & El-Sherbiny, S. A. (2016). An overview of production and development of ceramic membranes. *International Journal of Applied Engineering Research*, *11*(12), 7708-7721.

Bae, B. U., Jung, Y. H., Han, W. W., & Shin, H. S. (2002). Improved brine recycling during nitrate removal using ion exchange. *Water Research*, *36*(13), 3330-3340.

Baker, R. W. (2004). Membrane technology and applications. *Membrane Technology*.

Bandini, S., & Vezzani, D. (2003). Nanofiltration modeling: the role of dielectric exclusion in membrane characterization. *Chemical engineering science* , *58* (15), 3303-3326.

Bargeman, G., Westerink, J. B., Manuhutu, C. F. H., & ten Kate, A. (2015). The effect of membrane characteristics on nanofiltration membrane performance during processing of practically saturated salt solutions. *Journal of membrane science*, *485*, 112-122.

Beetstra, R., Lafont, U., Nijenhuis, J., Cellar, EM, & van Ommen, JR (2009). Atmospheric pressure process for coating particles using atomic layer deposition. *Chemical Vapor Deposition* , *15*(7-9), 227-233.

Bhattacharjee, S. (2017). Concentration Polarization: Early Theories. WATER PLANET.

Bian, R., Yamamoto, K., & Watanabe, Y. (2000). The effect of shear rate on controlling the concentration polarization and membrane fouling. *Desalination* , *131* (1-3), 225-236.

Calmon, C. (1986). Recent developments in water treatment by ion exchange. *Reactive Polymers, Ion Exchangers, Sorbents* , *4*(2), 131-146.

Calvo, J. I., Bottino, A., Capannelli, G., & Hernández, A. (2008). Pore size distribution of ceramic UF membranes by liquid–liquid displacement porosimetry. *Journal of Membrane Science*, *310*(1-2), 531-538.

Cao, GZ, Meijernik, J., Brinkman, HW, & Burggraaf, AJ (1993). Permporometry study on the size distribution of active pores in porous ceramic membranes. *Journal of membrane science* , *83*(2), 221-235.

Chang, Q., Zhou, J.E., Wang, Y., Liang, J., Zhang, X., Cerneaux, S., Wang, X., Zhu, Z. and Dong, Y., 2014. Application of ceramic microfiltration membrane modified by nano-TiO2 coating in separation of a stable oil-in-water emulsion. *Journal of Membrane Science*, *456*, 128-133.

Chen, H., Jia, X., Wei, M., & Wang, Y. (2017). Ceramic tubular nanofiltration membranes with tunable performances by atomic layer deposition and calcination. *Journal of Membrane Science* , *528* , 95-102.

Chen, H., Wu, S., Jia, X., Xiong, S. and Wang, Y. (2018). Atomic layer deposition fabricating of ceramic nanofiltration membranes for efficient separation of dyes from water. *AIChE Journal*, 64(7), 2670-2678.

Chung, Y., Yun, Y. M., Kim, Y. J., Hwang, Y. S., & Kang, S. (2018). Preparation of alumina-zirconia (Al-Zr) ceramic nanofiltration (NF) membrane for the removal of uranium in aquatic system. *Water Science and Technology: Water Supply*, ws2018123.

Ciora, R.J. and Liu, P.K., (2003). Ceramic membranes for environmental related applications. *Fluid/Particle Separation Journal*, *15*(1), pp.51-60.

Cleanflow. (2018). *ceramic hollow fiber*. [online] Available at: https://www.cleanflowfilter.nl/en/ceramic-membrane-filter/ceramic-hollow-eiber-2/ [Accessed 17 Nov. 2018].

Comsol.asia. (2018). *Diffusion Coefficient Definition*. [online] Available at: https://www.comsol.asia/multiphysics/diffusion-coefficient [Accessed 1 Oct. 2018].

Condom, S., Larbot, A., Younssi, SA, & Persin, M. (2004). Use of ultra-and nanofiltration ceramic membranes for desalination. *Desalination* , *168* , 207-213.

Cornelissen, E., Moreau, N., Siegers, W., Abrahamse, A., Rietveld, L., Grefte, A., Dignum, M., Amy, G., and Wessels, L. (2008): Selection of anionic exchange resins for removal of natural organic matter (NOM) fractions, *Water Res., 42(1-2),* 413–423.

Cui, J., Zhang, X., Liu, H., Liu, S. and Yeung, K.L., 2008. Preparation and application of zeolite/ceramic microfiltration membranes for treatment of oil contaminated water. *Journal of Membrane Science*, *325*(1), 420-426.

D. van Halem, W. van der Meer, J. P. van der Hoek, L. Rietveld, B. Heijman, and M. Keuten, *"Nanofiltration and Reverse Osmosis," Drink. Water Treat. TU Delft Lect. Notes*, pp. 95–108, 2009.

David, F., Vokhmin, V., & Ionova, G. (2001). Water characteristics depend on the ionic environment. Thermodynamics and modelisation of the aquo ions. *Journal of Molecular Liquids*, *90*(1-3), 45-62.

De Lara, R., & Benavente, J. (2009). Use of hydrodynamic and electrical measurements to determine protein fouling mechanisms for microfiltration membranes with different structures and materials. *Separation and Purification Technology*, *66*(3), 517-524.

Déon, S., Dutournie, P., Fievet, P., Limousy, L., & Bourseau, P. (2013). Concentration polarization phenomenon during the nanofiltration or multi-ionic solutions: Influence of the filtrated solution and operating conditions. *Water research* , *47* (7), 2260-2272.

Déon, S., Dutournié, P., Limousy, L., & Bourseau, P. (2009). Transport of salt mixtures through nanofiltration membranes: numerical identification of electric and dielectric contributions. *Separation and Purification Technology*, *69*(3), 225-233.

Donnan, F. G. (1995). Theory of membrane equilibria and membrane potentials in the presence of non-dialysing electrolytes. A contribution to physical-chemical physiology. *Journal of Membrane Science*, *100*(1), 45-55.

Drikas, M., Dixon, M., & Morran, J. (2011). Long term case study of MIEX pre-treatment in drinking water; understanding NOM removal. *Water research*, *45*(4), 1539-1548.

Erdem, ©. (2017, February). Sol-gel applications for ceramic membrane preparation. In *AIP Conference Proceedings*(Vol.1809, No. 1, p.020011). AIP Publishing.

Fan, PM, Zhen, KF, Zan, ZY, Chao, Z., Jian, Z., & Yun, JZ (2016). Preparation and development of porous ceramic membrane supports fabricated by extrusion technique. *Chemical Engineering Transactions* , *55* , 277-282.

Fang, J., & Deng, B. (2014). Rejection and modeling of arsenate by nanofiltration: Contributions of convection, diffusion and electromigration to arsenic transport. *Journal of Membrane Science*, *453*, 42-51.

George, S. M. (2009). Atomic layer deposition: an overview. *Chemical reviews*, *110*(1), 111-131.

Ghalavand, Y., Hatamipour, M. S., & Rahimi, A. (2015). A review on energy consumption of desalination processes. *Desalination and Water Treatment*, *54*(6), 1526-1541.

Gilron, J., Gara, N., & Kedem, O. (2001). Experimental analysis of negative salt rejection in nanofiltration membranes. *Journal of Membrane Science*, *185*(2), 223-236.

Grefte, A., Dignum, M., Cornelissen, ER, & Rietveld, LC (2013). Natural organic matter removal at different positions in the drinking water treatment lane. *Drinking Water Engineering and Science* , *6* (1), 1-10.

Hagmeyer, G., & Gimbel, R. (1999). Modeling the rejection of nanofiltration membranes using zeta potential measurements. *Separation and purification technology* , *15* (1), 19-30.

Havel, J., & Högfeldt, E. (1995). Evaluation of water sorption equilibrium data on Dowex ion exchanger using WSLET-MINUIT program. *Scripta Fac. Sci. Wet. Univ. Masaryk. Brun. Chem* , *25*, 73-84.

Hofs, B., Ogier, J., Vries, D., Beerendonk, E. F., & Cornelissen, E. R. (2011). Comparison of ceramic and polymeric membrane permeability and fouling using surface water. *Separation and Purification Technology*, *79*(3), 365-374.

Horányi, G. (2003). Investigation of the specific adsorption of sulfate ions on powdered TiO2. *Journal of colloid and interface science*, *261*(2), 580-583.

http://www.sxceramic.com/. (2018). *Ceramic membrane*. [online] Available at: http://www.sxceramic.com/ceramic-membrane.html [Accessed 17 Nov. 2018].

Huber, SA, Balz, A., Abert, M., & Pronk, W. (2011). Characterization of aquatic humic and non-humic matter with size-exclusion chromatography-organic carbon detection-organic nitrogen detection (LC-OCD-OND). *Water research* , *45* (2), 879-885.

Hurwitz, G., Guillen, G. R., & Hoek, E. M. (2010). Probing polyamide membrane surface charge, zeta potential, wettability, and hydrophilicity with contact angle measurements. *Journal of Membrane Science*, *349*(1-2), 349-357.

Johnson, R. W., Hultqvist, A., & Bent, S. F. (2014). A brief review of atomic layer deposition: from fundamentals to applications. *Materials today*, *17*(5), 236-246.

Karnik, B. S., Davies, S. H., Baumann, M. J., & Masten, S. J. (2005). Fabrication of catalytic membranes for the treatment of drinking water using combined ozonation and ultrafiltration. *Environmental science & technology*, *39*(19), 7656-7661.

Kazarinov, VE, Andreev, VN, & Mayorov, AP (1981). Investigation of the adsorption properties of the TiO2 electrode by the radioactive tracer method. *Journal of Electroanalytical Chemistry and Interfacial Electrochemistry* , *130* , 277-285.

Kelewou, H., Lhassani, A., Merzouki, M., Drogui, P., & Sellamuthu, B. (2011). Salts retention by nanofiltration membranes: Physicochemical and hydrodynamic approaches and modeling. *Desalination*, *277*(1-3), 106-112.

Kestin, J., Khalifa, HE, & Correia, RJ (1981). Tables of the dynamic and kinematic viscosity of aqueous KCl solutions in the temperature range 25-150 C and the pressure range 0.1-35 MPa. *Journal of Physical and Chemical Reference Data* , *10* (1), 57-70.

Khalili, M., Sabbaghi, S., & Zerafat, MM (2015). Preparation of ceramic γ-Al 2 O 3-TiO 2 nanofiltration membranes for desalination. *Chemical Papers* , *69* (2), 309-315.

Khemakhem, S. and Amara, R.B., (2012). Purification of industrial effluent by microfiltration and ultrafiltration ceramic membranes: comparative study between commercial and elaborated Tunisian clay membranes. *Desalination and Water Treatment*, *39*(1-3), pp.182-189.

Kim, J., & Van der Bruggen, B. (2010). The use of nanoparticles in polymeric and ceramic membrane structures: review of manufacturing procedures and performance improvement for water treatment. *Environmental Pollution*, *158*(7), 2335-2349.

Koutsonikolas, D., Kaldis, S., Sakellaropoulos, GP, Van Loon, MH, Dirrix, RW, & Terpstra, RA (2010). Defects in microporous silica membranes: Analysis and repair. *Separation and Purification Technology* ,

Krieg, HM, Modise, SJ, Keizer, K., & Neomagus, HWJP (2005). Salt rejection in nanofiltration for single and binary salt mixtures in view of sulphate removal. *Desalination* ,

Kulkarni, V. S. (2009). *Handbook of non-invasive drug delivery systems: science and technology*. Elsevier.

Lee, M., Wu, Z., & Li, K. (2015). Advances in ceramic membranes for water treatment. In *Advances in Membrane Technologies for Water Treatment* (pp. 43-82).

Lee, S. J., Dilaver, M., Park, P. K., & Kim, J. H. (2013). Comparative analysis of fouling characteristics of ceramic and polymeric microfiltration membranes using filtration models. *Journal of Membrane Science*, *432*, 97-105.

Lee, S., & Cho, J. (2004). Comparison of ceramic and polymeric membranes for natural organic matter (NOM) removal. *Desalination*, *160*(3), 223-232.

Lee, S., Park, G., Amy, G., Hong, S. K., Moon, S. H., Lee, D. H., & Cho, J. (2002). Determination of membrane pore size distribution using the fractional rejection of nonionic and charged macromolecules. *Journal of Membrane Science*, *201*(1-2), 191-201.

Lee, SJ, & Kim, JH (2014). Differential natural organic matter fouling or ceramic versus polymeric ultrafiltration membranes. *Water research* , *48* , 43-51.

Li, F., Li, L., Liao, X., & Wang, Y. (2011). Precise pore size tuning and surface modifications of polymeric membranes using the atomic layer deposition technique. *Journal of membrane science*, *385*, 1-9.

Li, F., Yang, Y., Fan, Y., Xing, W., & Wang, Y. (2012). Modification of ceramic membranes for pore structure tailoring: The atomic layer deposition route. *Journal of membrane science* , *397* , 17-23.

Luque, S., Gómez, D. and Álvarez, J.R., 2008. Industrial Applications of Porous Ceramic Membranes (Pressure-Driven Processes). *Membrane Science and Technology*, *13*, pp.177-216.

Mazzoni, C., Orlandini, F., & Bandini, S. (2009). Role of electrolyte type on TiO2–ZrO2 nanofiltration membranes performances. *Desalination*, *240*(1-3), 227-235.

Meihong, L., Sanchuan, Y., Yong, Z., & Congjie, G. (2008). Study on the thin-film composite nanofiltration membrane for the removal of sulfate from concentrated salt aqueous: Preparation and performance. *Journal of Membrane Science*, *310*(1-2), 289-295.

Merdaw, A. A., Sharif, A. O., & Derwish, G. A. W. (2010). Water permeability in polymeric membranes, Part I. *Desalination*, *260*(1-3), 180-192.

Mullet, M., Fievet, P., Reggiani, JC, & Pagetti, J. (1997). Surface electrochemical properties or mixed oxide ceramic membranes: Zeta-potential and surface charge density. *Journal of Membrane Science* ,

Mustafa, G., Wyns, K., Buekenhoudt, A., & Meynen, V. (2016). New insights into the fouling mechanism of dissolved organic matter applying nanofiltration membranes with a variety of surface chemistries. *Water research*, *93*, 195-204.

Narayan, R., Adiga, S., Pellin, M., Curtiss, L., Stafslien, S., Chisholm, B., Monteiro-Riviere, N., Brigmon, R. and Elam, J. (2010). Atomic layer deposition of nanoporous biomaterials. *Materials Today*, *13*(3), 60-64.

Nghiem, L. D., & Hawkes, S. (2009). Effects of membrane fouling on the nanofiltration of trace organic contaminants. *Desalination*, *236*(1-3), 273-281.

Nicolini, J. V., Borges, C. P., & Ferraz, H. C. (2016). Selective rejection of ions and correlation with surface properties of nanofiltration membranes. *Separation and Purification Technology*, *171*, 238-247.

Nikkola, J., Sievänen, J., Raulio, M., Wei, J., Vuorinen, J., & Tang, C. Y. (2014). Surface modification of thin film composite polyamide membrane using atomic layer deposition method. *Journal of Membrane Science*, *450*, 174-180.

Pages, N., Yaroshchuk, A., Gibert, O., & Cortina, J. L. (2013). Rejection of trace ionic solutes in nanofiltration: Influence of aqueous phase composition. *Chemical engineering science*, *104*, 1107-1115.

Park, N., Kwon, B., Sun, M., Ahn, H., Kim, C., Kwoak, C., Lee, D., Chae, S., Hyung, H. and Cho, J. (2005). Application of various membranes to remove NOM typically occurring in Korea with respect to DBP, AOC and transport parameters. *Desalination*, 178(1-3),161-169.

Pérez-González, A., Ibáñez, R., Gómez, P., Urtiaga, A. M., Ortiz, I., & Irabien, J. A. (2015). Nanofiltration separation of polyvalent and monovalent anions in desalination brines. *Journal of Membrane Science*, *473*, 16-27.

Perry, M., & Linder, C. (1989). Intermediate reverse osmosis ultrafiltration (RO UF) membranes for concentration and desalting of low molecular weight organic solutes. *Desalination* , *71* (3), 233-245.

Poupeleer, A. S., Carmeliet, J., Roels, S., & Van Gemert, D. (2003). Bestimmung des Koeffizienten der Salzdiffusion in porösen Werkstoffen/Validation of the Salt Diffusion Coefficient in Porous Materials. *Restoration of Buildings and Monuments*, *9*(6), 663-682.

Puhlfürß, P., Voigt, A., Weber, R., & Morbé, M. (2000). Microporous TiO2 membranes with a cut off< 500 Da. *Journal of Membrane Science*, *174*(1), 123-133.

Qiu, M, Chen, X, Fan, Y, and Xing, W. (2017). Ceramic Membranes, *Comprehensive membrane science and engineering II. Elsevier.*

Rajasulochana, P., & Preethy, V. (2016). Comparison on efficiency of various techniques in treatment of waste and sewage water-A comprehensive review. *Resource-Efficient Technologies* , *2* (4), 175-184.

Rezakazemi, M., Sadrzadeh, M., & Matsuura, T. (2018). Thermally stable polymers for advanced high-performance gas separation membranes. *Progress in Energy and Combustion Science*, *66*, 1-41.

Sagle, A., & Freeman, B. (2004). Fundamentals of membranes for water treatment. *The future of desalination in Texas* , *2* (363), 137.

Salmenhaara, O. (2016). Separation of ions from acid solutions by nanofiltration.

Schaep, J., Van der Bruggen, B., Vandecasteele, C., & Wilms, D. (1998). Influence or ion size and charge in nanofiltration. *Separation and Purification Technology* , *14* (1-3), 155-162.

Schaep, J., Vandecasteele, C., Peeters, B., Luyten, J., Dotremont, C., & Roels, D. (1999). Characteristics and retention properties of a mesoporous γ-Al2O3 membrane for nanofiltration. *Journal of Membrane Science*, *163*(2), 229-237.

Schäfer, AI, Fane, AG, & Waite, TD (Eds.). (2005). *Nanofiltration: principles and applications* . Elsevier.

Schippers, D., Kooi, M., Sjoerdsma, P., & De Bruijn, F. (2005). Colour removal by ion exchange and reuse of regenerant by means of nanofiltration. *Water Science and Technology: Water Supply*, *4*(5-6), 57-64.

Shang, R. (2014). *Ceramic ultra-and nanofiltration for municipal wastewater reuse* (Doctoral dissertation, TU Delft, Delft University of Technology).

Shang, R., Goulas, A., Tang, C. Y., de Frias Serra, X., Rietveld, L. C., & Heijman, S. G. (2017). Atmospheric pressure atomic layer deposition for tight ceramic nanofiltration membranes: Synthesis and application in water purification. *Journal of Membrane Science*, *528*, 163-170.

Shang, R., Verliefde, A., Hu, J., Zeng, Z., Lu, J., Kemperman, A., Deng, H., Nijmeijer, K., Heijman, S. and Rietveld, L.(2014). Tight ceramic UF membrane as RO pre-treatment: The role of electrostatic interactions on phosphate rejection. *Water research*, *48*, 498-507.

Shang, R., Vuong, F., Hu, J., Li, S., Kemperman, A., Nijmeijer, K., Cornelissen, E., Heijman, S. and Rietveld, L.. (2015). Hydraulically irreversible fouling on ceramic MF/UF membranes: Comparison of fouling indices, foulant composition and irreversible pore narrowing. *Separation and purification technology*, *147*, 303-310.

Siddiqui, M.U., Arif, A.F.M. and Bashmal, S., 2016. Permeability-selectivity analysis of microfiltration and ultrafiltration membranes: Effect of pore size and shape distribution and membrane stretching. *Membranes*, *6*(3), p.40.

Silva, V., Montalvillo, M., Carmona, F. J., Palacio, L., Hernández, A., & Prádanos, P. (2016). Prediction of single salt rejection in nanofiltration membranes by independent measurements. *Desalination*, *382*, 1-12.

Skluzacek, J. M., Tejedor, M. I., & Anderson, M. A. (2007). NaCl rejection by an inorganic nanofiltration membrane in relation to its central pore potential. *Journal of membrane science*, *289*(1-2), 32-39.

Sondhi, R., Bhave, R. and Jung, G., 2003. Applications and benefits of ceramic membranes. *Membrane Technology*, *2003*(11), pp.5-8.

Song, Z., Fathizadeh, M., Huang, Y., Chu, K., Yoon, Y., Wang, L., Xu, W. and Yu, M. (2016). TiO 2 nanofiltration membranes prepared by molecular layer deposition for water purification. *Journal of Membrane Science*, *510*, 72-78.

Sun, X., Wu, J., Chen, Z., Su, X., & Hinds, B. J. (2013). Fouling characteristics and electrochemical recovery of carbon nanotube membranes. *Advanced Functional Materials*, *23*(12), 1500-1506.

Szoke, S., Patzay, G., & Weiser, L. (2003). Characteristics of thin-film nanofiltration membranes at various pH-values. *Desalination*, *151*(2), 123-129.

Szymczyk, A., & Fievet, P. (2006). Ion transport through nanofiltration membranes: the steric, electric and dielectric exclusion model. *Desalination*, *200*(1-3), 122-124.

Tadros, T. (2014). Colloid and interface aspects of pharmaceutical science. In *Colloid and Interface Science in Pharmaceutical Research and Development* (pp. 29-54).

Tan, X., & Li, K. (2013). Dense ceramic membranes for membrane reactors. In *Handbook of Membrane Reactors: Fundamental Materials Science, Design and Optimisation* (pp. 271-297).

Tan, X., Liu, Y., & Li, K. (2005). Mixed conducting ceramic hollow-fiber membranes for air separation. *AIChE journal*, *51*(7), 1991-2000.

Tanganov, BB (2013). About size of the hydrated salt ions-the component of sea water. *European Journal of Natural History.*

Tannins, J., Mänttäri, M., & Nyström, M. (2006). Effect of salt mixture concentration on fractionation with NF membranes. *Journal of Membrane Science* , *283* (1-2), 57-64.

Tansel, B. (2012). Significance of thermodynamic and physical characteristics on permeation of ions during membrane separation: Hydrated radius, hydration free energy and viscous effects. *Separation and purification technology*, *86*, 119-126.

Tansel, B., Sager, J., Rector, T., Garland, J., Strayer, R., Levine, L., Roberts, M., Hummerick, M. and Bauer, J. (2006). Significance of hydrated radius and hydration shells on ionic permeability during nanofiltration in dead end and cross flow modes. *Separation and Purification Technology*, *51*(1), 40-47.

Tsuru, T., Hironaka, D., Yoshioka, T., & Asaeda, M. (2001). Titania membranes for liquid phase separation: effect of surface charge on flux. *Separation and Purification Technology*, *25*(1-3), 307-314.

Tu, NP (2013). Role of Charge Effect During Membrane Filtration.

Van Gestel, T., Vandecasteele, C., Buekenhoudt, A., Dotremont, C., Luyten, J., Leysen, R., Van der Bruggen, B. and Maes, G. (2002). Alumina and titania multilayer membranes for nanofiltration: preparation, characterization and chemical stability. *Journal of membrane Science* , *207* (1), 73-89.

Vaudevire, E., Koreman, E. (2013). Ion exchange brine treatment: closing the loop of NaCl use and reducing disposal towards a zero liquid discharge.

Verberk, JQJC (2005). Application of air in membrane filtration. *Pasmans Offsetdrukkerij bv, Gravenhage* .

Vezzani, D., & Bandini, S. (2002). Donnan equilibrium and dielectric exclusion for characterization of nanofiltration membranes. *Desalination* , *149* (1-3), 477-483.

Vitagliano, V., & Lyons, P. A. (1956). Diffusion coefficients for aqueous solutions of sodium chloride and barium chloride. *Journal of the American Chemical Society*, *78*(8), 1549-1552.

Voigt, I., Stahn, M., Junghans, A., Rost, J., & Voigt, W. (2001). Integrated cleaning of coloured waste water by ceramic NF membranes. *Separation and Purification Technology*, *25*(1-3), 509-512.

Wang, D. X., Su, M., Yu, Z. Y., Wang, X. L., Ando, M., & Shintani, T. (2005). Separation performance of a nanofiltration membrane influenced by species and concentration of ions. *Desalination*, *175*(2), 219-225.

Web.mit.edu. (2018). *LEMI: Laboratory for Energy and Microsystems Innovation at MIT | Research: Electrokinetics*. [online] Available at: http://web.mit.edu/lemi/rsc_electrokinetics.html [Accessed 17 Nov. 2018].

Weber, M., Julbe, A., Ayral, A., Miele, P., & Bechelany, M. (2018). Atomic layer deposition for membranes: Basics, challenges and opportunities. *Chemistry of Materials*.

Weber, R., Chmiel, H., & Mavrov, V. (2003). Characteristics and application of new ceramic nanofiltration membranes. *Desalination*, *157*(1-3), 113-125.

Wesselingh, J. A., & Krishna, R. (2000). *Mass transfer in multicomponent mixtures* (pp. 46-54). Delft: Delft University Press.

Winter, J., Barbeau, B., & Bérubé, P. (2017). Nanofiltration and Tight Ultrafiltration Membranes for Natural Organic Matter Removal—Contribution of Fouling and Concentration Polarization to Filtration Resistance. *Membranes*, *7*(3), 34.

Yaldız, S. (2017). *Application of tubular ceramic nanofiltration membranes for textile waste water desalination* (Master's thesis, İzmir Institute of Technology).

Yan, Z. Q., Zeng, L. M., Li, Q., Liu, T. Y., Matsuyama, H., & Wang, X. L. (2016). Selective separation of chloride and sulfate by nanofiltration for high saline wastewater recycling. *Separation and Purification Technology*, *166*, 135-141.

Yoon, S. H. (2015). *Membrane bioreactor processes: principles and applications*. CRC press.

Zhao, K., & Li, Y. (2006). Dielectric characterization of a nanofiltration membrane in electrolyte solutions: Its double-layer structure and ion permeation. *The Journal of Physical Chemistry B*, *110*(6), 2755-2763.

Zhao, Y., Xing, W., Xu, N. and Wong, F.S., (2005). Effects of inorganic electrolytes on zeta potentials of ceramic microfiltration membranes. *Separation and Purification Technology*, *42*(2), pp.117-121.